

MINIMIZING AXIS DRIFT IN FULLY COMPLIANT SLIDER-CRANK
MECHANISM

A THESIS SUBMITTED TO
THE GRADUATE SCHOOL OF NATURAL AND APPLIED SCIENCES
OF
MIDDLE EAST TECHNICAL UNIVERSITY

BY

UFUK ENES SAYGILI

IN PARTIAL FULFILLMENT OF THE REQUIREMENTS
FOR
THE DEGREE OF MASTER OF SCIENCE
IN
MECHANICAL ENGINEERING

JANUARY 2023

Approval of the thesis:

**MINIMIZING AXIS DRIFT IN A FULLY COMPLIANT SLIDER-CRANK
MECHANISM**

submitted by **Ufuk Enes SAYGILI** in partial fulfillment of the requirements for the degree of **Master of Science in Mechanical Engineering, Middle East Technical University** by,

Prof. Dr. Halil Kalipçılar
Dean, Graduate School of **Natural and Applied Sciences** _____

Prof. Dr. M. A. Sahir Arıkan
Head of the Department, **Mechanical Engineering** _____

Prof. Dr. Yiğit Yazıcıoğlu
Supervisor, **Mechanical Engineering, METU** _____

Dr. Erdinç N. Yıldız
Co-Supervisor, **Ekinoks-AG Inc.** _____

Examining Committee Members:

Assoc. Prof. Dr. M. Bülent Özer
Mechanical Engineering Dept., METU _____

Prof. Dr. Yiğit Yazıcıoğlu
Mechanical Engineering Dept., METU _____

Assist. Prof. Dr. Gökhan Osman Özgen
Mechanical Engineering Dept., METU _____

Prof. Dr. Engin Tanık
Mechanical Engineering Dept., Hacettepe University _____

Prof. Dr. Gökhan Kiper
Mechanical Engineering Dept., İzmir Institute of Technology _____

Date: 23.01.2023

I hereby declare that all information in this document has been obtained and presented in accordance with academic rules and ethical conduct. I also declare that, as required by these rules and conduct, I have fully cited and referenced all material and results that are not original to this work.

Name, Last name: Ufuk Enes Saygılı

Signature:

ABSTRACT

MINIMIZING AXIS DRIFT IN FULLY COMPLIANT SLIDER-CRANK MECHANISM

Saygılı, Ufuk Enes
Master of Science, Mechanical Engineering
Supervisor: Prof. Dr. Yiğit Yazıcıoğlu
Co-Supervisor: Dr. Erdiñ N. Yıldız

January 2023, 85 pages

Compliant slider-crank mechanisms have been studied several times to gain the advantages of compliant mechanisms. The advantages of compliant mechanisms are precision, reducing cost, having no wear, and reducing weight, all gained by manufacturing them as a single piece without backlash. Compliant slider-crank mechanisms also have a critical disadvantage to solve: axis drift and axis rotation of the output segment. Partially compliant slider-cranks are studied several times, and there is only one study on a fully-compliant slider-crank mechanism, but this mechanism has a considerable axis drift which is not desired motion of slider-crank. This study proposes a fully compliant slider-crank mechanism with minimized axis drift and the largest possible stroke. Proposed mechanism is observed kinematically with the help of pseudo-rigid-body model. A force analysis is conducted with virtual work method. Theoretical solution is verified with finite element analysis and measurements of the manufactured prototype of the proposed mechanism.

Keywords: Compliant Mechanisms, Slider-Crank Mechanisms, Minimized Axis Drift

ÖZ

TAMAMEN ESNEK BİR KRANK-BİYEL MEKANİZMASINDA EKSEN KAYMASINI EN AZA İNDİRMEK

Saygılı, Ufuk Enes
Yüksek Lisans, Makina Mühendisliği
Tez Yöneticisi: Prof. Dr. Yiğit Yazıcıoğlu
Ortak Tez Yöneticisi: Dr. Erdiç N. Yıldız

Ocak 2023, 85 sayfa

Esnek krank-biyel mekanizmaları, esnek olmalarının sağladıkları avantajları elde etmek amacıyla birçok kez çalışılmıştır. Esnek mekanizmaların avantajları; hassaslık, düşük maliyet, sürtünmesizlik, hafiflik olarak sıralanabilir ve bu avantajlar mekanizmaların boşluksuz olarak tek parça olarak üretilmeleri sayesinde elde edilir. Esnek krank-biyel mekanizmalarının dezavantajı ise kızak üzerindeki eksen kayması ve eksen dönmesidir. Kısmen esnek krank-biyel mekanizmaları üzerine birçok çalışma bulunmakta ama tamamıyla esnek krank-biyel mekanizması üzerine sadece bir çalışma bulunmaktadır. Bu mekanizmada krank-biyel mekanizmalarında istenmeyen bir hareket olan kayda değer ölçüde eksen kayması vardır. Bu tez kapsamında, kızak hareketini en yüksek seviyede tutarak eksen kaymasını en aza indirgeyecek bir esnek krank-biyel mekanizması tasarlanmaktadır. Tasarlanan mekanizma PRBM yardımı ile kinematik olarak incelenmektedir. Virtual iş metodu kullanılarak kuvvet analizi gerçekleştirilmiştir. Sonlu elemanlar analizi ve üretilen prototip üzerindeki ölçümler ile teorik çözüm doğrulanmıştır.

Anahtar Kelimeler: Esnek Mekanizmalar, Krank-Biyel Mekanizmaları, Azaltılmış Eksen Kayması,

To my lovely family

ACKNOWLEDGMENTS

I would like to express my appreciation to my supervisor Prof. Dr. Yiğit Yazıcıoğlu for his support, valuable comments and contributions to complete this thesis.

I would like to express my special thanks to my co-supervisor Dr. Erdinç N. Yıldız for his patience, criticism and supervision during this study. He has been a master for me with his wisdom, intelligence and engineering knowledge.

I would like to express my gratitude to my sisters Ayça and Esmâ for their truthful support and trust. I would like to specially thank to my mother Zübeyde for her endless love, patience and encouragement throughout my all life.

I would like to express my special appreciation to my brother Mustafa for his moral support and brotherhood throughout my life. I will always feel his support behind me and never forget his cheerful face.

Lastly, I am grateful to my wife İlkay for the inspiration and support she provided throughout my work. Expressing my feelings to her is very difficult for an engineer. Without her loving encouragement, understanding and positive energy, it would have been impossible for me to complete this work. Very special thanks to her for being part of my life.

TABLE OF CONTENTS

ABSTRACT.....	v
ÖZ	vi
ACKNOWLEDGMENTS	viii
TABLE OF CONTENTS.....	ix
LIST OF TABLES	xii
LIST OF FIGURES	xiii
LIST OF ABBREVIATIONS	xvi
CHAPTERS	
1 INTRODUCTION	1
1.1 Motivation.....	1
1.2 Objective	2
1.3 Organization of the Thesis	2
2 LITERATURE REVIEW	5
2.1 History of Compliant Mechanisms	5
2.2 Compliant Slider-Crank Mechanisms.....	6
2.3 Joints and Joint Types	10
2.4 Double-Parallelogram Flexure Mechanisms.....	12
3 COMPLIANT MECHANISM FUNDAMENTALS	17
3.1 Strength and Stiffness	17
3.2 Flexural Segment Stiffness	18

3.3	PRBM.....	22
3.4	Material Selection.....	23
4	DESIGN OF THE MECHANISM	27
4.1	Introduction	27
4.2	Design of Small-Length Flexure	29
4.3	Proposed Mechanism.....	32
4.4	PRBM.....	34
4.5	Kinematic Solution	36
4.6	Dimensions of Proposed Mechanism	40
4.7	Kinematic Simulation.....	41
4.8	Virtual Work Method	47
5	FINITE ELEMENTS ANALYSES AND RESULTS.....	55
5.1	Analysis with 1D Elements	55
5.2	Analysis with 3D Elements	62
5.2.1	Analysis Details	63
5.2.2	Results.....	64
6	EXPERIMENTS.....	69
6.1	Manufacturing Process	69
6.2	Test Setup	70
6.3	Test Results	71
6.4	Comparison.....	72
7	CONCLUSIONS	77
	REFERENCES	79

APPENDICES

A. CoC of Polypropylene.....83

B. Screenshot of Measurement with CMM84

C. Dimensions of the Mechanism (All dimensions are in mm)85

LIST OF TABLES

TABLES

Table 3.1 Ratio of yield strength to Young's modulus for several materials [2]	24
Table 4.1 Pseudo-rigid link angle and stiffness values of SLF	31
Table 4.2 Kinematic Results of the Mechanism.....	46
Table 5.1 Results of FEA with 1D Elements	61
Table 5.2 Results of FEA with 3D Elements	68
Table 6.1 Measurement Results of Prototype for desired Angle of Crank	71
Table 6.2 Comparison of Stroke Values of mechanism	72
Table 6.3 Comparison of Axis Drift Values of mechanism	74
Table 6.4 Comparison of Axis Rotation Values of the Mechanism.....	75

LIST OF FIGURES

FIGURES

Figure 2.1. Sketch of compliant catapult [2].....	6
Figure 2.2. Prototype of slider crank flexible mechanism prepared for	7
Figure 2.3. Compliant slider-crank mechanism of Pardeshi et al. [7]	8
Figure 2.4. Proposed constant force mechanism in [8].....	8
Figure 2.5. Undeformed and current position of slider-crank mechanism [9]	9
Figure 2.6. (a) PRBM (b) isometric view of the mechanism whose slider is composed of fixed guided compliant segment[10]	10
Figure 2.7. Benchmarked flexible translational joints [11]	11
Figure 2.8. Prototype of the spatial compliant translational joint manufactured by 3D printing [12]	12
Figure 2.9. Typical double-parallelogram flexure [15].....	13
Figure 2.10. Double-parallelogram flexure [14].....	13
Figure 2.11. Nested underconstraint eliminator linkage [16]	14
Figure 2.12. Flexure double-parallelogram with nested underconstraint eliminator linkage [17]	15
Figure 3.1. Cantilever beam.....	17
Figure 3.2. PRBM model of small-length flexural pivot.....	19
Figure 3.3. (a) A compliant four-bar mechanism and its (b) PRBM [2].....	23
Figure 4.1. Flow chart for a compliant mechanism design process [20]	28
Figure 4.2. Dimensions of proposed SLF	29
Figure 4.3. Meshing of SLF	30
Figure 4.4. Front and isometric view of mechanism	32
Figure 4.5. Double-Parallelogram Flexure	33
Figure 4.6. Double-Parallelogram Compliant Mechanism	34
Figure 4.7. PRBM of the mechanism.....	35
Figure 4.8. PRBM of the deformed mechanism	35
Figure 4.9. Position of Link 2 and Link 3	39

Figure 4.10. Dimensions of Proposed Mechanism.....	41
Figure 4.11. Results of kinematic analysis (Initial state)	42
Figure 4.12. Results of kinematic analysis (3° CCW).....	42
Figure 4.13. Results of kinematic analysis (3° CW)	43
Figure 4.14. Results of kinematic analysis (6° CCW).....	43
Figure 4.15. Results of kinematic analysis (6° CW)	44
Figure 4.16. Results of kinematic analysis (9° CCW).....	44
Figure 4.17. Results of kinematic analysis (9° CW)	45
Figure 4.18. Results of kinematic analysis (12° CCW).....	45
Figure 4.19. Results of kinematic analysis (12° CW)	46
Figure 4.20. Loop of Virtual Work Method	47
Figure 4.21. Difference Between θ_{16} and θ_{18} vs Links Lengths Ratio.....	52
Figure 4.22. Axis Drift vs Links Lengths Ratio	53
Figure 4.23. Stroke vs Links Lengths Ratio	53
Figure 5.1. Representation of Elements and Boundary Conditions	56
Figure 5.2. Results of stroke analysis with 1D elements (3° right)	57
Figure 5.3. Results of stroke analysis with 1D elements (3° left)	57
Figure 5.4. Results of stroke analysis with 1D elements (6° right)	58
Figure 5.5. Results of stroke analysis with 1D elements (6° left)	58
Figure 5.6. Results of stroke analysis with 1D elements (9° right)	59
Figure 5.7. Results of stroke analysis with 1D elements (9° left)	60
Figure 5.8. Results of stroke analysis with 1D elements (12° right)	60
Figure 5.9. Results of stroke analysis with 1D elements (12° left)	61
Figure 5.10. Analysis flow chart	62
Figure 5.11. Mesh and Boundary Conditions of 3D Model	63
Figure 5.12. Results of stroke analysis with 3D elements (3° CCW) (mm).....	64
Figure 5.13. Results of stroke analysis with 3D elements (3° CW) (mm)	64
Figure 5.14. Results of stroke analysis with 3D elements (6° CCW) (mm).....	65
Figure 5.15. Results of stroke analysis with 3D elements (6° CW) (mm)	65
Figure 5.16. Results of stroke analysis with 3D elements (9° CCW) (mm).....	66

Figure 5.17. Results of stroke analysis with 3D elements (9° CW) (mm).....	66
Figure 5.18. Results of stroke analysis with 3D elements (12° CCW) (mm)	67
Figure 5.19. Results of stroke analysis with 3D elements (12° CW) (mm).....	67
Figure 6.1. CAD model of mechanism for experiments.	69
Figure 6.2. Test Setup	70
Figure 6.3. Comparison of Stroke Results of FEA and Experiment.....	73
Figure 6.4. Comparison of Axis Drift Results of FEA and Experiment.....	74
Figure 6.5. Comparison of Axis Rotation Results of FEA and Experiment.....	76

LIST OF ABBREVIATIONS

ABBREVIATIONS

1D	One Dimensional
2D	Two Dimensional
3D	Three Dimensional
CCW	Counterclockwise
COC	Certificate of Conformity
CW	Clockwise
FEA	Finite Element Analysis
PRBM	Pseudo-Rigid-Body Model
SLF	Small Length Flexure
T1	Translation in X Direction
T2	Translation in Y Direction
T3	Translation in Z Direction
R1	Rotation about X Axis
R2	Rotation about Y Axis
R3	Rotation about Z Axis

CHAPTER 1

INTRODUCTION

1.1 Motivation

Most machines need a mechanism to complete its task. The abilities and performance of mechanisms strongly affect the efficiency and capabilities of machines. Therefore, mechanical engineers are always interested in mechanisms. Traditional rigid-body mechanisms consisting of rigid links connected with movable joints have been studied for a long time. With the advancement of manufacturing technologies, the efficiency and reliability of mechanisms increased to an acceptable level.

Compliant mechanisms that have flexible components are becoming more popular because of their nature that is manufactured as single or fewer parts. Their advantages of cost reduction; reduced number of parts, more straightforward manufacturing process, simplistic assembly and improved performance, more reliable and precise motion, reduced wear, easy and less frequent maintenance make them more attractive for engineers.

The theory and application have been well developed with the research conducted by the academia and industry over the previous few decades. As a result, there are now much more products whose functionality depend on flexible members. The fields of MEMS, adaptive and smart structures, robotics, precision engineering, micro and nano gadgets, medical devices, handheld equipment, and everyday products all use a variety of compliant mechanism designs. The study of compliant mechanisms will advance when more sophisticated materials are created [1].

On the other side of advantages of compliant mechanisms, they are complex during the analysis and synthesis. Researchers should build and solve nonlinear equations. Solving these nonlinear equations needs more mathematical knowledge,

computational power and time. The design procedure needs too much iteration to reach the final geometry.

1.2 Objective

This thesis aims to design, analyze and test a fully compliant slider-crank mechanism with minimized axis drift. A translational joint to slider link must be added to reduce axis drift. This study focuses on the adaptation of prismatic joint to the slider link.

1.3 Organization of the Thesis

The outline of thesis is presented shortly as follows:

In Chapter 2, a literature review on compliant mechanisms is conducted. This chapter contains a general literature review about flexible mechanisms, and a more specific review of literature about compliant slider-crank mechanisms. Also there is a section in this chapter which presents studies about flexible double parallelograms.

In Chapter 3, mathematical background and essential preliminary information are explained. This chapter explains PRBM method, flexibility and deflection and material selection procedure.

In Chapter 4, the design steps and details of the mechanism are explained. Kinematic analysis and results of the proposed mechanism and a solid model of the mechanism is also presented in this chapter.

In Chapter 5, analysis and results of the mechanism are presented. Including analysis with 1D elements and 3D elements, two FEA simulations are conducted. The result of the analysis is presented and tabulated. Comments and comparisons are made on the results.

In Chapter 6, the manufacturing process of the proposed mechanism, the test setup, the test process and the test results are presented.

Finally, in Chapter 7, main findings of study are concluded, and future works are suggested.

CHAPTER 2

LITERATURE REVIEW

Mechanisms are used to transfer or transform energy, motion or force. Traditional mechanisms consist of rigid links and movable joints. By contrast, compliant mechanisms gain their all or some of the motion from the deflection of flexible joints rather than rigid joints [2]. The advantages of compliant mechanisms can be separated into two main categories: reduced cost of manufacturing and improved performance, having no backlash in the joints and being manufactured as a single piece [2]. The main area of application of compliant mechanisms is where precision and predictability are required.

Compliant mechanisms would undergo large deflections to transfer or transform motion and large deflection of beams needs to be solved nonlinearly, making design and analysis of compliant mechanisms harder than traditional ones. There are opportunities to solve large deflection problems like finite element models, nonlinear shooting methods and the elliptic integral solutions [3]. The pseudo-rigid-body model (PRBM) is a practical tool for analyzing compliant mechanisms by the knowledge of rigid-body kinematics. A torsional spring is added to flexible beams to simulate the stored energy when they deflect, guaranteeing the accuracy in a range of deflection.

2.1 History of Compliant Mechanisms

Flexible members have been used as a part of mechanism or machines for millennia. Archaeologists say that flexible bows have been used since 8000 B.C. [2]. These bows are generally made of wood and animal strew.

There are a lot of examples of flexible mechanisms in history. People used tweezers in predynastic Egypt. There are a lot of figures that show Egyptians holding materials with tweezers. Another example of flexible machines is catapults. The Greeks used compliant members as early as the fourth century B.C., as shown by the employment of catapults [2]. Early models of catapults are generally wooden. In Figure 2.1, a sketch of Leonardo Davinci's catapult design is showed.

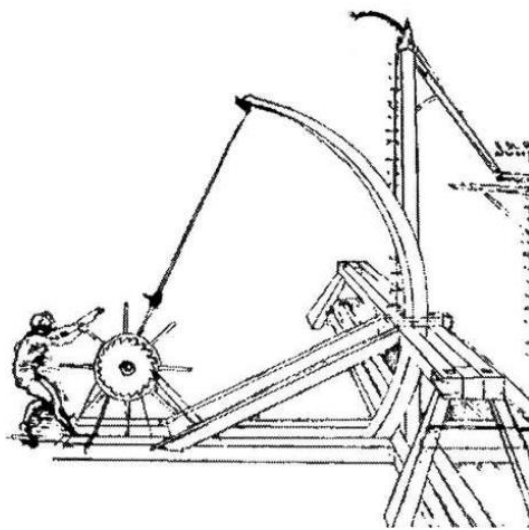


Figure 2.1. Sketch of compliant catapult [2]

2.2 Compliant Slider-Crank Mechanisms

Different mechanisms are studied to design or analyze compliant versions of them. Liu et al. [4] proposed model and design for constant-force gripper based on buckled fixed-guided beams. This mechanism utilizes positive and negative stiffness mechanisms to gain constant force output. The function of the negative-stiffness part is achieved by using the buckling effect of the inclined beam. Dao and Huang [5] presented the optimal design and formulation of a kinematic model of a flexible slider-crank mechanism (Figure 2.2). They used flexible beams as revolute joints,

but for prismatic joints they used a traditional model. They used PRDM in this study. They also focused on increasing fatigue life of the mechanism.

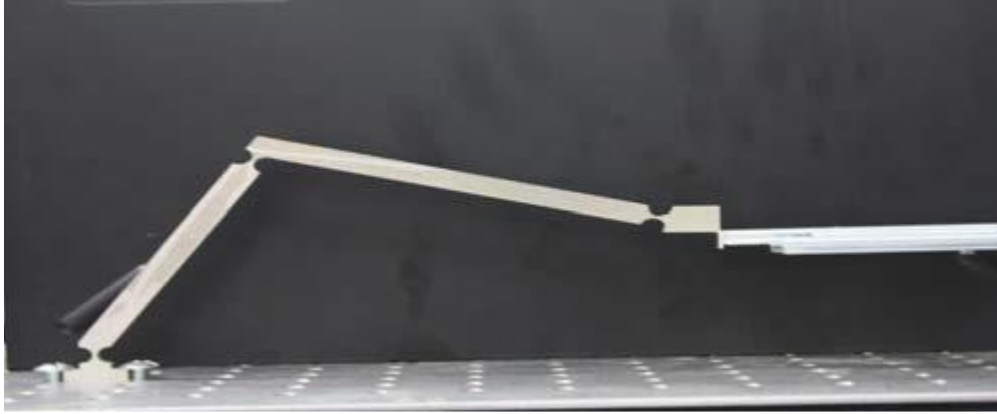


Figure 2.2. Prototype of slider crank flexible mechanism prepared for kinematic and dynamic testing [5]

Bilancia et al. [6] worked on the design of a long-stroke beam-based compliant mechanism providing quasi-constant force. A flexure-based slider-crank mechanism is designed, and its dimensions are optimized for quasi-constant force.

Pardeshi et al. [7] developed a model for a monolithic compliant slider-crank mechanism (Figure 2.3). The purpose of the mechanism is motion amplification. They manufactured a model after design and FEA results are nearly identical to experimental results.

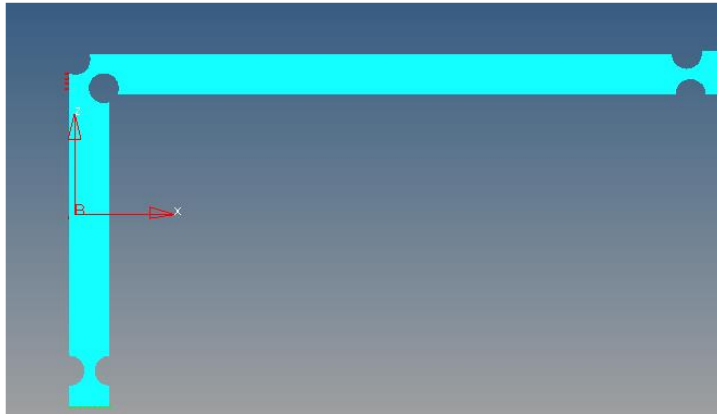


Figure 2.3. Compliant slider-crank mechanism of Pardeshi et al. [7]

Tolman et al. [8] proposed a fully compliant constant force mechanism that uses an initially angled parallel-guiding mechanism. Mechanism is calculated first by PRBM and validated by FEA and experimental setup.

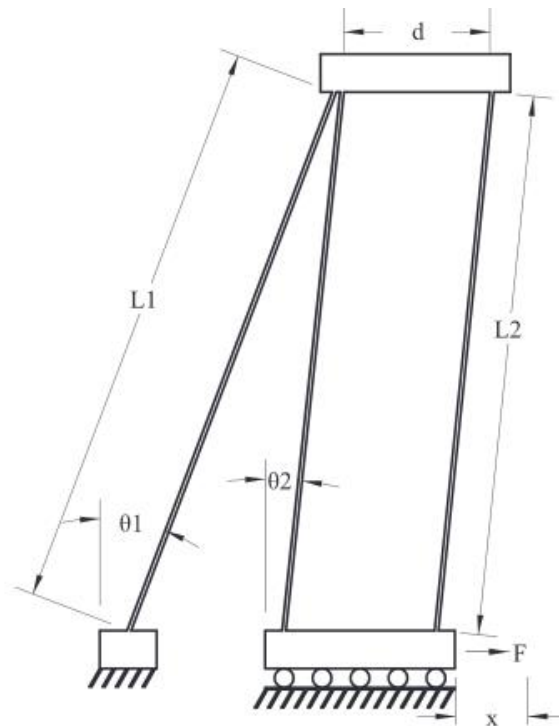


Figure 2.4. Proposed constant force mechanism in [8]

Parklataş and Tanık [9] conducted a study on a single piece compliant spatial slider-crank mechanism (Figure 2.5). Since the mechanism is spatial, torsional springs in the flexible revolute joints, deflections at the multiple axis flexural hinges are used for bending and twisting separately. Transformation matrices are generated for bending and twisting modes of flexible parts. An experimental fatigue setup is prepared for design. No indication of failure is observed after 1.5 million cycles.

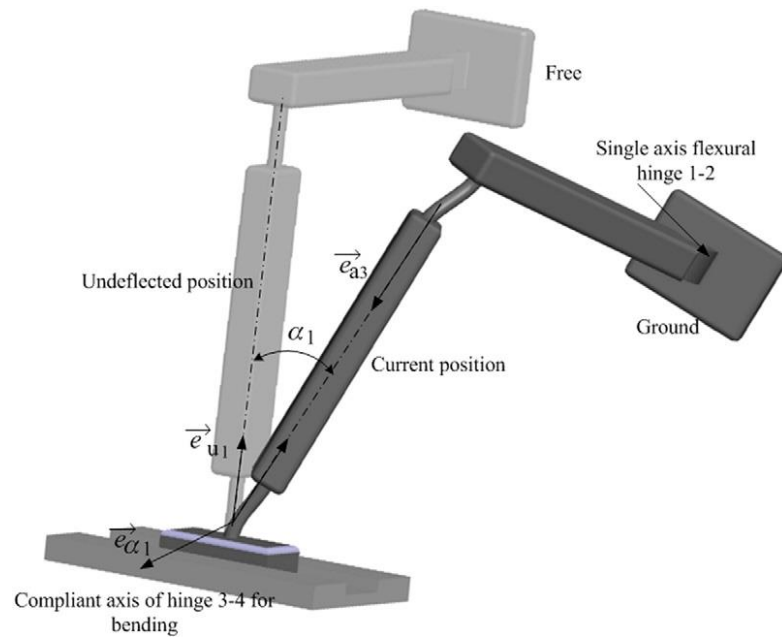


Figure 2.5. Undeformed and current position of slider-crank mechanism [9]

Tanık et al. [10] proposed a fully compliant planar slider-crank mechanism (Figure 2.6). This design is the first example of a fully compliant planar slider-crank mechanism in the literature. Fully compliant mechanisms gain their all mobility from compliance of its body, they do not contain any conventional joints. 2 fixed guided segments are used to compose a prismatic joint. Fixed guided links and slider segment are analyzed as a parallelogram loop which are shown in Figure 2.6. A kinematic approach is the first step in examining this mechanism. Then torsional stiffness elements are added to the system to add an effect of stored energy. The

mechanism utilizes a long range for slider link with help of the parallelogram, but the main disadvantage of the parallelograms is the curvilinear motion characteristics. The curvilinear motion of parallelogram brings considerable axis drift to the mechanism.

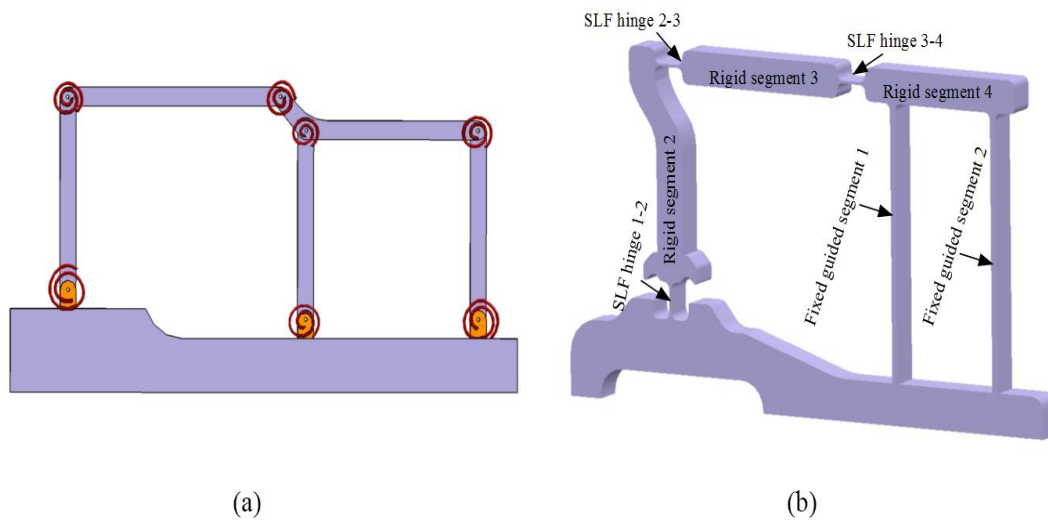


Figure 2.6. (a) PRBM (b) isometric view of the mechanism whose slider is composed of fixed guided compliant segment[10]

2.3 Joints and Joint Types

Treesa et al. [11] developed compliant large displacement joints. This study offers many models for large-displacement translational and revolute joints. Models are compared by the range of motion, axis drift, stress concentration, off-axis stiffness and compactness (Figure 2.7). The study also provides a formulation for axis stiffness and off-axis stiffness.

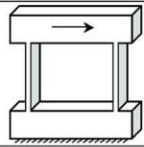
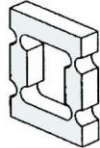
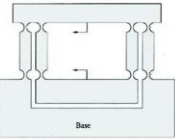
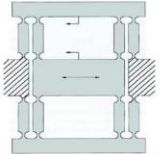
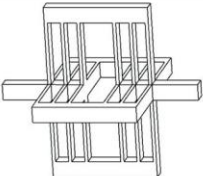
		Range of Motion	Axis Drift	Stress Concentration	Off-Axis Stiffness	Compactness
(a)		0	-	0	0	+
(b)		-	-	-	0	+
(c)		-	0	-	0	+
(d)		-	+	-	0	+
(e)		+	+	+	+	+

Figure 2.7. Benchmarked flexible translational joints [11]

Yang et al. [12] studied the design of a spatial compliant prismatic joint (Figure 2.8). The paper presents a compliant prismatic joint with significant stiffness and slight axis drift. Many positions are analyzed, and a three-dimensional construction is proposed. Axial and rotational stiffness values for compliant translational joints are calculated.

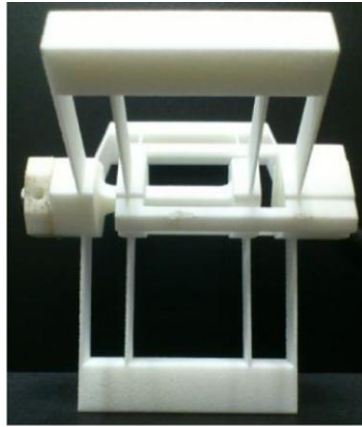


Figure 2.8. Prototype of the spatial compliant translational joint manufactured by 3D printing [12]

2.4 Double-Parallelogram Flexure Mechanisms

Double-parallelogram flexures were studied several times in the literature. The advantages of being easy to analyze and synthesize make the double-parallelogram mechanism an excellent option for compliant mechanisms. Compared to a single parallelogram flexure connection, the double-parallelogram structure increases the range and reduces kinematic errors for its main translation degree-of-freedom (DOF) [13], [14].

The double-parallelogram mechanism cannot work correctly without joint clearances, but compliant ones can operate by compliance of flexure elements. Yangmin and Qingsong [15] used double-parallelogram mechanism as an element of XY stage with decoupled motion mechanism (Figure 2.9). They used different combinations and types of double parallelograms for different conceptual designs.

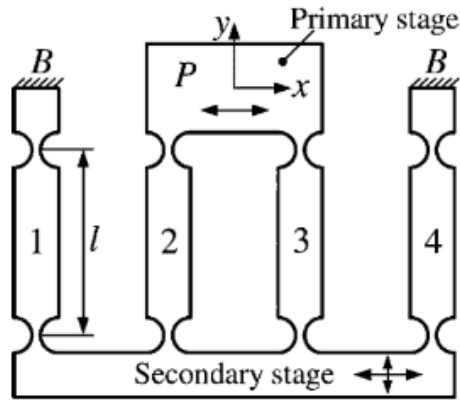


Figure 2.9. Typical double-parallelogram flexure [15]

Awtar et al. [14] proposed a non-dimensional method to estimate the performance characteristics of a beam flexure mechanism (Figure 2.10). They studied the effects of load-stiffening and elastokinematic nonlinearities in beams. They applied the theory to parallel and double-parallelogram mechanisms and compared these mechanisms in terms of their transverse and axial stiffness.

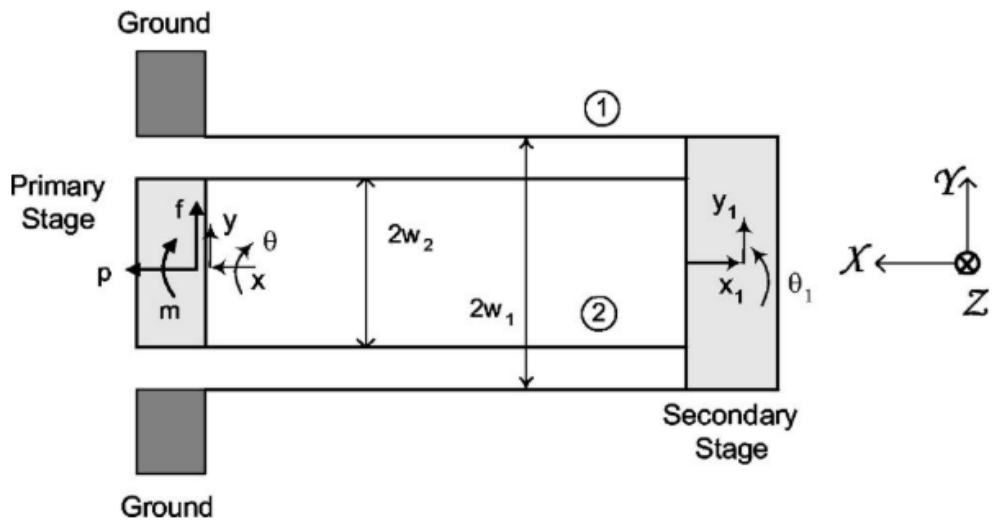


Figure 2.10. Double-parallelogram flexure [14]

Awtar et al. [14] applied their method to a parallelogram flexure. They observed that axial deflection of flexure beams is independent of axial force and does not contribute to axial rotation but it makes a contribution to axis drift. After application of this method to double-parallelogram flexure, they observed that if there is no axial load and a y-displacement is applied to the primary stage, the transverse stiffness values for the two parallelograms are equal, and y-displacement is consequently distributed evenly between the stages where primary stage and coordinates are expressed in Figure 2.10.

Panas [16] created an analytical method that estimates the large displacement behaviour of flexural double parallelogram bearings with an underconstraint eliminator (Figure 2.11). A model is used to understand the motion and characteristics of underconstraint eliminator. He focused on the effect of underconstraint eliminator linkage on y-axis stiffness of a double-parallelogram flexure. The method utilizes the design of underconstraint eliminators.

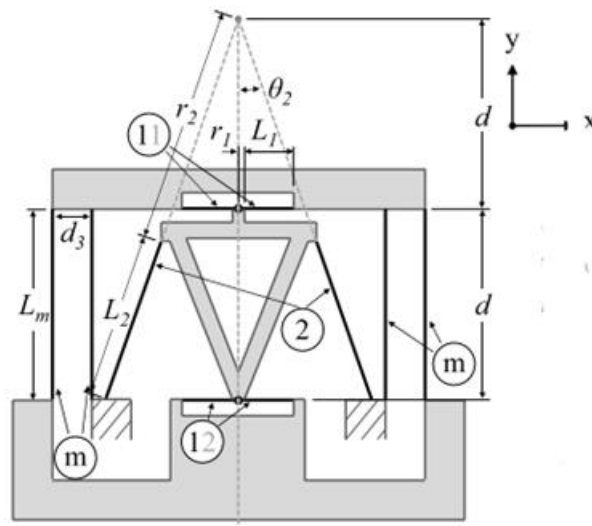


Figure 2.11. Nested underconstraint eliminator linkage [16]

Panas and Hopkins [17] proposed a flexural linkage design for removing underconstraint in a double-parallelogram. With the additional linkage, most static

and dynamic problems are solved. They compare their underconstraint eliminator with the ones in the literature. This link makes the resonance frequency of the double-parallelogram 11 times higher and eliminates underconstraint. Modified double-parallelogram of Panas and Hopkins are shown in Figure 2.12.

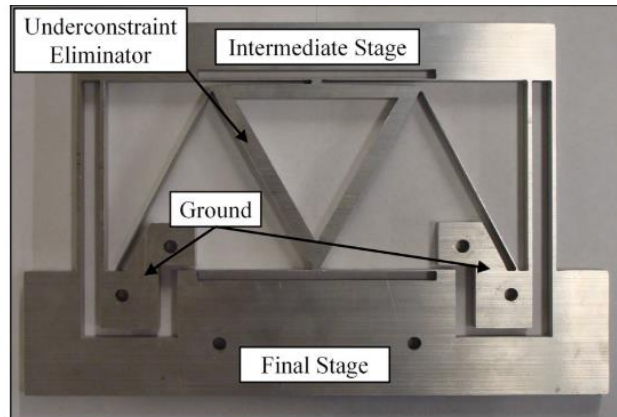


Figure 2.12. Flexure double-parallelogram with nested underconstraint eliminator linkage [17]

Hopkins and Panas [18] conducted a study that introduces a family of flexible linkages that can be used to avoid underconstraint for nested and large-stroke flexible systems.

CHAPTER 3

COMPLIANT MECHANISM FUNDAMENTALS

3.1 Strength and Stiffness

A material's degree of deformation under a specific load is influenced by its stiffness. Strength, on the other hand, describes the highest stress that a material can bear before failing [2].

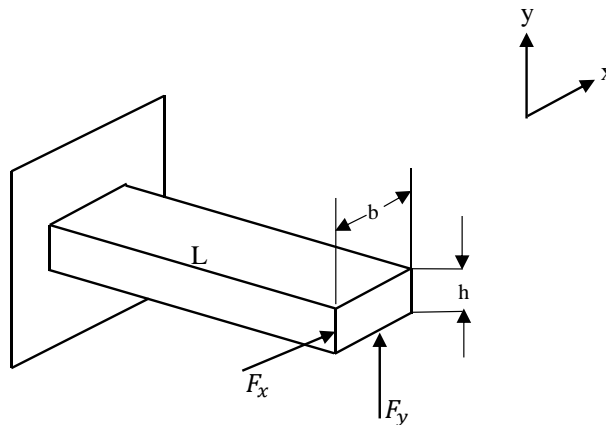


Figure 3.1. Cantilever beam

Stiffness of a mechanical element is dependent on both geometry and material properties. Flexural stiffness, which is for bending case of loading, is given by EI , where E is modulus of elasticity and I is cross-sectional moment of inertia. Axial stiffness is given by EA , where A is area of cross-section.

Consider a beam fixed at one end as shown in Figure 3.1. The material is a predefined isotropic material, i.e. the properties of the material are equal for every direction. For a beam the inertia is much larger in one axis. When force in x -direction, F_x , deflects

the material until the maximum stress reaches yield strength of the material, the deflection S can be calculated as;

$$\delta_x = \frac{2SL^2}{3Eb} \quad 3-1$$

Similarly, the maximum deflection before failure in the y-direction can be calculated as

$$\delta_y = \frac{2SL^2}{3Eh} \quad 3-2$$

The relation of maximum deflections in x- and y-directions can be related as

$$\delta_x = \frac{h}{b} \delta_y \quad 3-3$$

The material has equal strength in both directions, but Equation 3-3 clearly shows that the stiffness of the structure is different in different directions.

3.2 Flexural Segment Stiffness

Compliant mechanisms generally use flexural segments for the revolute joints. Flexural segments are short beams that can have large deflections compared with their length.

A beam with two segments, one of which is short and flexible in bending directions and the other is longer and rigid in those directions, can be described as a small-

length flexural pivot. Given that the tiny segment is both shorter and more flexible than the large segment, the following requirements can be used to characterize the segment's structure [2]. A conceptual drawing of PRBM of flexural segment is shown in Figure 3.2.

$$L \gg l \quad 3-4$$

$$(EI)_L \gg (EI)_l \quad 3-5$$

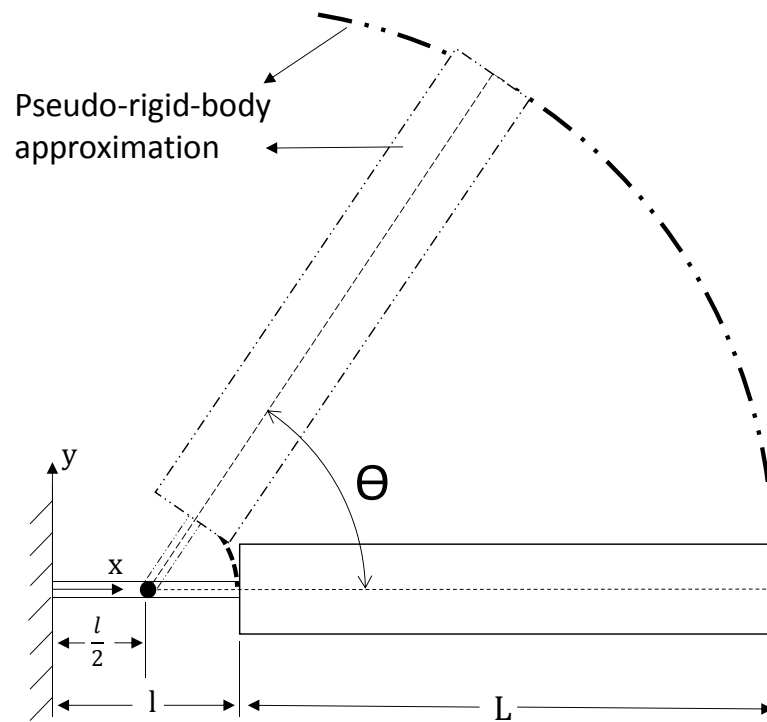


Figure 3.2. PRBM model of small-length flexural pivot

The following deflection equations are developed for the flexible section with end moment loading [2]:

$$\theta_0 = \frac{M_0 l}{EI} \quad 3-6$$

$$\frac{\delta_y}{l} = \frac{1 - \cos\theta_0}{\theta_0} \quad 3-7$$

$$\frac{\delta_x}{l} = 1 - \frac{\sin\theta_0}{\theta_0} \quad 3-8$$

The motion of the system can be represented as two rigid links connected at a pin joint, called the characteristic pivot, because the flexible part is significantly shorter than the rigid section. The characteristic pivot is located at the center of the flexural pivot, as shown in Figure 3.2. This assumption is correct since the deflection occurs at the flexible segment and it is small relative to the rigid section's length. For the same reason, the characteristic pivot may essentially be placed at any point along the flexible section, and the center point is only employed for convenience. θ , the pseudo-rigid-body angle, is the angle of the pseudo-rigid link. For small-length flexural pivots, the angle of pseudo-rigid-body is same with the angle at the beam end [2].

$$\theta = \theta_0 \quad 3-9$$

The approximate x- and y-coordinates of the beam's termination, denoted by a and b , are as follows:

$$a = \frac{l}{2} + \left(L + \frac{l}{2}\right) \cos\theta \quad 3-10$$

$$b = \left(L + \frac{l}{2}\right) \sin\theta \quad 3-11$$

Non-dimensional forms of the equations are:

$$\frac{a}{l} = \frac{l}{2} + \left(\frac{L}{l} + \frac{l}{2}\right) \cos\theta \quad 3-12$$

$$\frac{b}{l} = \left(\frac{L}{l} + \frac{l}{2}\right) \sin\theta \quad 3-13$$

Modelling of the beam's resistance to deflection uses a torsional spring with a K -valued spring constant. The torsional spring must be deflected with a torque T in order to rotate by an angle θ [2]:

$$T = k\theta \quad 3-14$$

The elementary beam theory can be used to calculate the spring constant, K . For a beam having a moment M at the end, the end angle is [2]

$$\theta_0 = \frac{Ml}{(EI)_l} \quad 3-15$$

To calculate M :

$$M = \frac{(EI)_l}{l} \theta_0 \quad 3-16$$

Using $M = T$ and $\theta_0 = \theta$, spring constant can be calculated as

$$k = \frac{(EI)_l}{l} \quad 3-17$$

If the primary loading on the flexural pivot is bending, then this model is more accurate. Higher error will be introduced into the model if the axial and transverse loads are greater than the bending moment. Main benefit of this model is that since there is no assumption about small deflection, there would be no error in large deflection cases [2].

3.3 PRBM

Pseudo-rigid-body models are useful tools to understand and visualize compliant mechanisms since models give an opportunity to model flexible bodies as rigid bodies. With this facility compliant mechanisms can be analyzed and synthesized [19].

PRBM is a bridge that makes rigid body mechanism theory and compliant mechanism theory. This model assumes a deflection path and a relationship between load and deflection. Flexure segments are modelled as revolute joints and a torsional spring on it. Specifying the revolute joint and stiffness of torsional spring is a critical step of pseudo-rigid-body models [2].

The design requirements and restrictions are examined to determine whether the pseudo-rigid-body mechanism satisfies them. The pseudo-rigid-body mechanism may be changed and reanalysed if they are not satisfied. Iterative techniques or

formal optimization procedures may be used in the loop involving modifying and analysing the pseudo-rigid-body mechanism. Quite often the designer may discover that the chosen sort of mechanism does not easily satisfy the design goals. In this case, a new rigid-body mechanism must be created, and the process must be repeated [20]. A four-bar mechanism and its PRBM is showed in Figure 3.3.

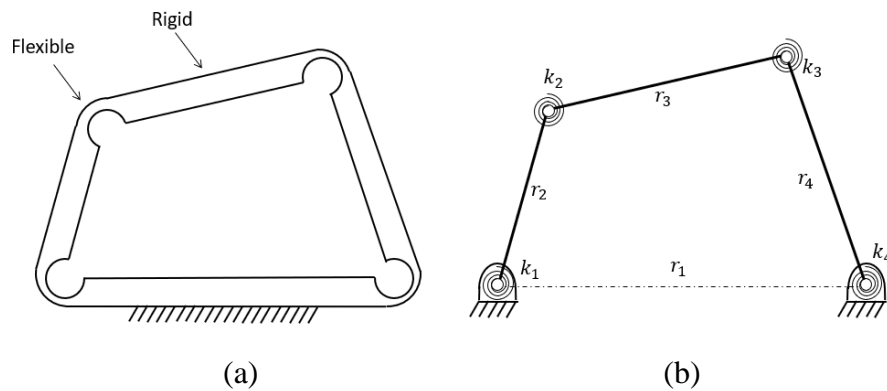


Figure 3.3. (a) A compliant four-bar mechanism and its (b) PRBM [2]

3.4 Material Selection

Material selection is a critical step for every engineering application. Compliant mechanism materials are also important for performance and life of mechanism. There are lots of material options for different compliant mechanism applications.

The most crucial thing to remember is that flexibility and strength can be combined. Additionally, brittle materials may be utilized to build compliant devices if their geometry is designed to prevent overstressing them. A part can be made more flexible by changing its geometry or material qualities.

Materials for compliant mechanisms are chosen to optimize flexibility rather than stiffness, unlike most other mechanical devices or structures. So, making

mechanisms more flexible while keeping it strong is a significant point of compliant mechanism design.

The ratio of yield strength to Young's modulus is a deterministic parameter for compliant mechanisms. This ratio shows how beams can deflect before they fail. This ratio is one of the most crucial factors to consider when choosing materials for applications using compliant mechanisms [2].

Table 3.1 Ratio of yield strength to Young's modulus for several materials [2]

Material	E (GPa)	S_y (MPa)	$S_y/E \times 1000$
Steel (1010 hot rolled)	207	179	0.87
Steel (4140 Q&TQ@400)	207	1641	7.9
Aluminum (1100 annealed)	71.7	34	0.48
Aluminum (7075 annealed)	71.7	503	7.0
Titanium (Ti-35A annealed)	114	207	1.8
Titanium (Ti-13 heal treated)	114	1170	10
Beryllium copper (CA 170)	128	1170	9.2
Polycrystalline silicon	169	930	5.5
Polyethylene (HDPE)	1.4	28	20
Nylon (type 66)	2.8	55	20
Polypropylene	1.4	34	25
Kevlar (82 vol %) in epoxy	86	1517	18
E-glass (73.3 vol %) in epoxy	56	1640	29

For various reasons, polypropylene is a frequently utilized polymer in compliant mechanisms. As may be seen in Table 3.1, it possesses a very high strength to modulus ratio. Compared to other polymers with comparable strength-to-modulus ratios, it also has several advantages. Low density, being affordable, widely accessible, and simple to process are the advantageous characteristics of

polypropylene. Additionally, it is extremely ductile and considerably less likely to yield in a disastrous way. Because the material must withstand significant strains for millions of cycles, this makes it an excellent choice for hinges. Consequently, polypropylene is appropriate for many compliant mechanisms [2].

CHAPTER 4

DESIGN OF THE MECHANISM

4.1 Introduction

The choice of the type of mechanism and the number of joints and links necessary for the mechanism to permit motion with a finite number of degrees of freedom are often covered by structural synthesis. Techniques for counting and detecting mechanisms have significantly benefited from the contributions of numerous writers [21].

All process of compliant mechanism design needs real attention. While a large translation is needed in the mechanism we developed for this study, protecting the mechanism from failure is the most important design constraint. A kinematics-based method is typically well suited for mechanisms that experience significant nonlinear deflections. In addition, this method needs to start with a rigid mechanism that is well established [22].

In the design, the main objective is to keep axis drift and axis rotation of slider minimum while keeping its range of translation maximum. The general approach for this purpose is to make the translational joint of slider less stiff in the direction of desired motion, which makes a more significant stroke, and make translational joint more rigid in the axis drift direction. For this purpose, a double-parallelogram mechanism is used to support translational motion of the slider link. Double-parallelogram mechanism has little stiffness in the translational motion direction of the slider link, and a considerable stiffness in the axis drift direction of slider link. With the benefits of double-parallelogram mechanism, proposed fully-compliant slider-crank mechanism achieves characteristic features of slider-crank mechanisms.

For design, analysis and test procedure, selected material is polypropylene. By this selection, advantages of polypropylene is gained which are explained in Chapter 3.4.

A design approach, which is proposed by Howell and Midha [20] is presented in Figure 4.1.

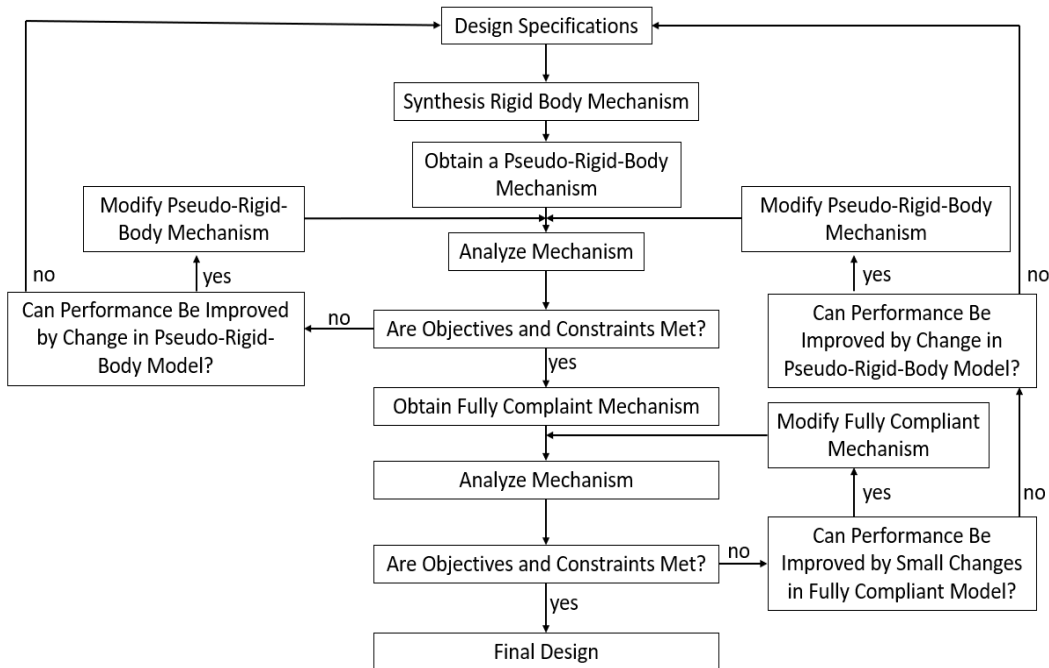


Figure 4.1. Flow chart for a compliant mechanism design process [20]

As seen in Figure 4.1, designing compliant mechanisms needs a lot of iteration. Suitable iterations can achieve desired characteristic features and requirements of design. After every design step, kinematic and finite element analysis steps must be conducted. According to the results of the analysis, required improvements should be implemented to design.

4.2 Design of Small-Length Flexure

In order to provide a small amount of angular motion about an axis, small-length flexure (SLF) is a mechanical component that takes the place of a revolute joint. The SLF is particularly energy-efficient since it has zero contact friction and backlash and is monolithic with the links it connects [23]. The main difference between SLF from classical revolute joints is their torsional spring behaviour. An SLF also has characteristics of a torsional spring along the desired axis of rotation [24]. The design procedure of compliant mechanisms needs to calculate the torsional spring constant of SLFs.

Since material of the mechanism is selected as polypropylene, material is used for the analysis and design of SLF.

An SLF design is proposed for implementation to design of compliant a slider-crank mechanism. Torsional spring constant of an SLF can be calculated by the equations given in Chapter 2. Figure 4.2 shows the dimensions of our proposed design.

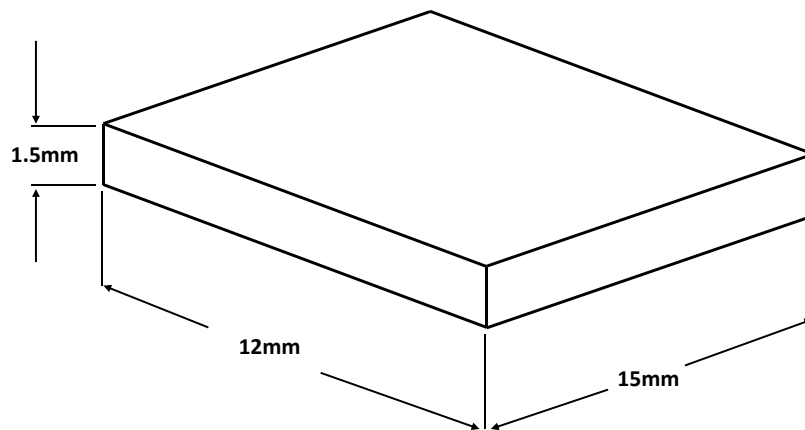


Figure 4.2. Dimensions of proposed SLF

$$I = \frac{bh^3}{12} = \frac{15 \text{ mm} \times (1.5 \text{ mm})^3}{12} = 4.22 \text{ mm}^4 \quad 4-1$$

$$k = \frac{EI}{l} = \frac{1400 \text{ MPa} \times 4.22 \text{ mm}^4}{12 \text{ mm}} = 492.19 \text{ N}\cdot\text{mm}/\text{rad} \quad 4-2$$

An FEA is conducted to validate the stiffness values of SLF. FEA also shows the linear stiffness characteristics of the SLF.

FEA is conducted with a 2D model of SLF with fillets of 3 mm. The 2D model is created on CAD software and imported to Patran. 2D quad elements are created based on the geometry of SLF as shown in Figure 4.3. Properties of polypropylene are assigned to the elements. Torque is applied to excite SLF. Torque is applied at the right side of SLF and the other side is fixed. To eliminate stress concentration at the corners, excitation and boundary faces are stretched 3 mm more to outside.

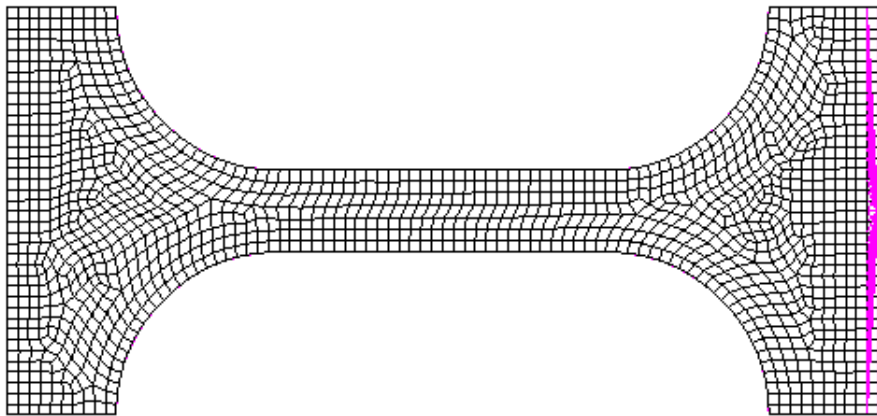


Figure 4.3. Meshing of SLF

From the displacement of nodes at the side where torque is applied, pseudo-rigid link angle, θ , is calculated as follows.

$$\theta = \arcsin \left(2 \frac{\Delta y}{l} \right) \quad 4-3$$

where l is the length of SLF and Δy is the displacement of nodes at the side torque applied. Pseudo-rigid link angle and stiffness values are derived from the results of FEA, and equations (3-14) and (4-3) are used for the derivation. Calculated values are showed in Table 4.1.

Table 4.1 Pseudo-rigid link angle and stiffness values of SLF

Torque ($N \square mm$)	Δy (mm)	θ (deg)	k ($N \square mm/rad$)
20	0.246	2.35	487.67
50	0.615	5.88	486.95
80	0.981	9.41	487.10
110	1.341	12.91	488.34
140	1.714	16.46	487.35
160	1.932	18.76	488.57

Torsional spring constant of SLF is calculated as $492.19 N \cdot mm/rad$ by equation (3-17). The average stiffness value derived from the displacement results of FEA is 487.52 . The difference between analytical results and FEA results is less than 1%.

Stiffness values of SLF in the range of 0° to 18.6° are nearly the same. The maximum difference between stiffness values is 0.2%, so it is clear that motion of SLF is almost linear in the range of motion.

Another consideration for SLF design must be stress levels on the SLF. From FEA results, stresses on SLF are observed for 8 cases of analysis. Maximum stress occurs at the 12° CCW case where the SLF connects the crank. Connecting link deflects nearly 44° , and stress is nearly 30 MPa. Since yield strength of polypropylene is 34 MPa, the proposed SLF design is safe for this motion.

Dimensions of SLF is arranged as the dimensions of proposed mechanism. Depth of SLF is fixed by the dimensions of links of mechanism. Other dimensions of the SLF are determined by stress and stiffness levels. As SLF becomes stiffer, moving the mechanism gets harder. As it becomes weaker, stress level would increase. An appropriate dimension set is determined by the comprehension of stress and stiffness.

Thus, the calculated stiffness value can be assigned to the torsional spring constant of revolute joints that represents the flexural hinges for the analysis of PRBM of the proposed mechanism.

4.3 Proposed Mechanism

A fully compliant slider-crank mechanism is designed with the knowledge mentioned in previous chapters. Slider-crank mechanism converts rotary motion of crank link to translational motion of slider link. The main objective of the proposed mechanism is to convert motion to a pure translational motion. To gain pure translational motion without axis drift and axis rotation on slider link, a double-parallelogram mechanism is used to act as a prismatic joint. Geometry of the proposed fully compliant slider-crank mechanism is given in Figure 4.4.

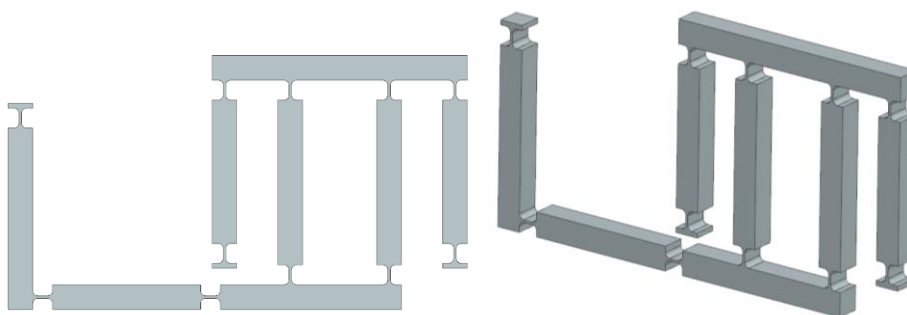


Figure 4.4. Front and isometric view of mechanism

Double-parallelogram flexural bearings are used commonly in devices where precision is desired [2], [13], [25] for several advantages of them. Double-parallelogram flexure and stages are shown in Figure 4.5. The double-parallelogram structure offers larger stroke and reduced off-axis motion for its translation motion DOF over a parallelogram flexural bearing [13], [14]. Single parallelogram flexure shows an elliptical motion. For a large displacement motion, this elliptical motion causes a considerable y-axis motion [16]. In double-parallelogram flexures, secondary stage shows the same y-axis motion but in the opposite direction. By the way, y-axis motion of stages cancel out in a double-parallelogram flexures.

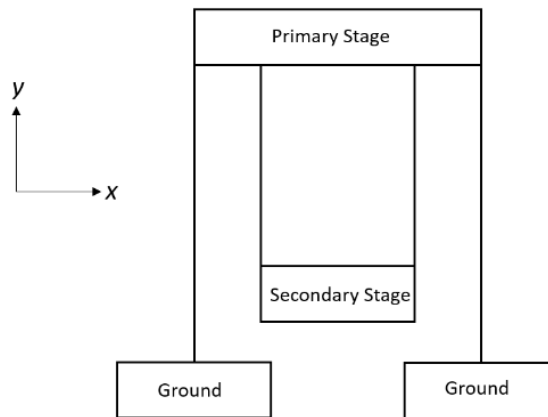


Figure 4.5. Double-Parallelogram Flexure

Hopkins and Culpepper mentioned advantages of serial flexure systems [26]. Double-parallelogram mechanism is a characteristic example of serial flexure systems. Larger strokes and less parasitic errors are the main advantages of serial flexures than parallel flexures. They also designated that cancelation of y-axis motion of two stages.

Double parallelogram flexure is studied before several times because of its advantages comes from its nature [2], [14], [16], [25], [27]. Studies focused on formulation of double-parallelogram flexures and its motion characteristics.

In this study, double-parallelogram mechanism is applied to a slider-crank mechanism as a translational joint which is shown in Figure 4.6. Double-parallelogram compliant mechanism differs from double-parallelogram flexures by its rigid guides and small length flexures instead of flexures. Small length flexures give compliance by behaving a revolute joint and torsional spring on it. This characteristic offers more robust and repeatable motion than long flexures. Before this study, there was no compliant slider-crank mechanism with a double-parallelogram mechanism. Throughout this study, the calculations and characteristics of this mechanism is concluded.

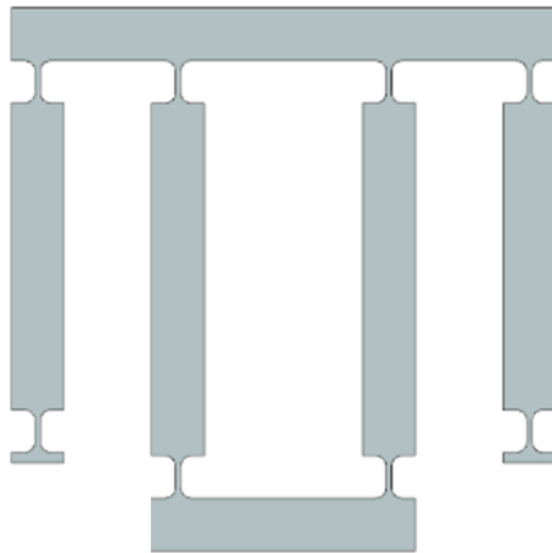


Figure 4.6. Double-Parallelogram Compliant Mechanism

4.4 PRBM

To accomplish compliant mechanism design, PRBM of desired model should be obtained. PRBM of compliant mechanisms generally includes rigid links and revolute joints with torsional springs.

PRBM of the proposed mechanism is given in Figure 4.7. Revolute joints are lumped as points at the middle of SLF, and lengths of rigid links are calculated as the distance between joints. PRBM of the deformed mechanism is illustrated in Figure 4.8.

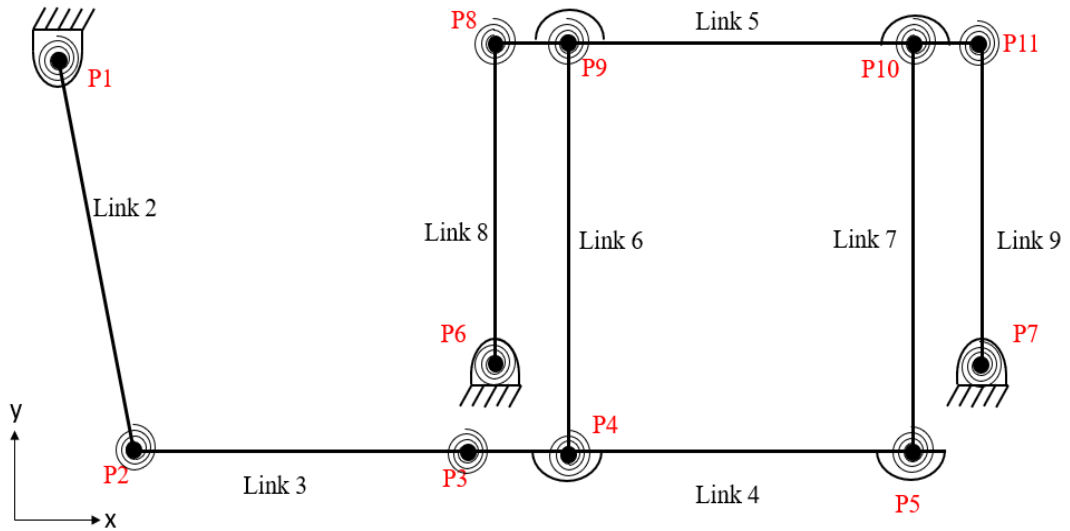


Figure 4.7. PRBM of the mechanism

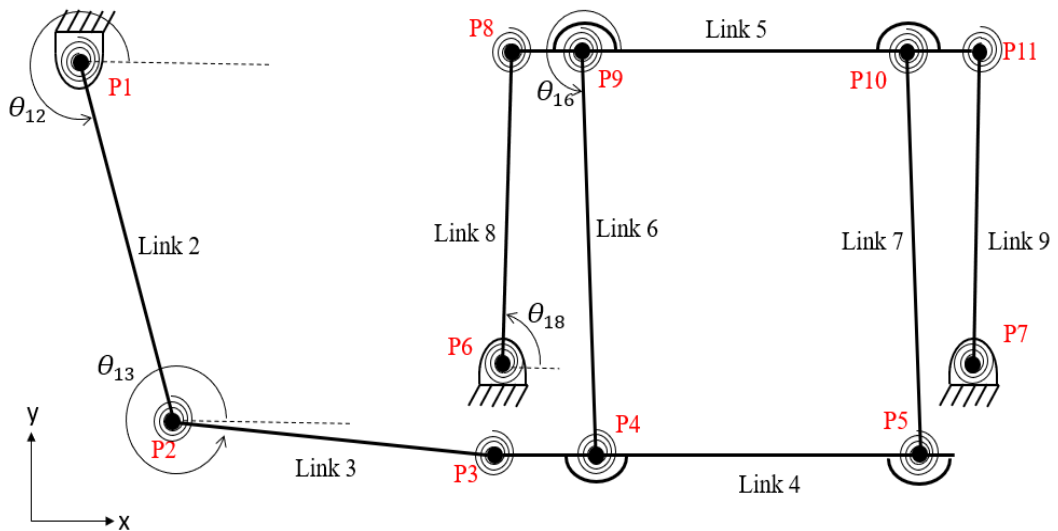


Figure 4.8. PRBM of the deformed mechanism

4.5 Kinematic Solution

Kinematic analysis of the PRBM of the mechanism should be conducted during design process. Basically, PRBM in Figure 4.7 is consist of as follows:

- Link 2 – Crank link (Input),
- Link 3 – Connecting link,
- Link 4 – Slider link (Output),
- Link 5, Link 6, Link 7, Link 8, Link 9 – Parts of double-parallelogram mechanism which acts as a prismatic joint.

A rotary motion on the input link is created by an applied torque on it. The mechanism converts this rotational motion into a translational motion on the slider part. The output of the mechanism could have translational motion against a force according to the needs of the application.

Kutzbach [13] criterion for DOF of a planar mechanism is

$$N = 3(l - 1) - 2j_1 - j_2 \quad 4-4$$

where l refers to the number of links (including ground), j_1 refers to the number of single DOF joints and j_2 refers to the number of two DOF joints. DOF of the mechanism is calculated as $N = 2$ by this criterion. The first kinematic approach of proposed mechanism would be as a classical mechanism with 2 inputs but then virtual work method is applied to proposed mechanism. Since compliant mechanism has a torsional spring on every revolute joint by its characteristic, mechanism could be driven with one input.

PRBM includes links, revolute joints and torsional springs. All the member of PRBM is shown in Figure 4.7. The revolute joints on P1, P6 and P7 are fixed to the ground. So these points cannot move during the motion of the mechanism. The positions of

these points are assumed to be known in the kinematic analysis. Lengths of all links are constant and known for this design and r_i represents length of i^{th} link.

The mechanism includes two parallelograms. The first one consists of Link 1, Link 8, Link 5 and Link 9 and the nature of being a parallelogram brings that $r_8 = r_9$. The second parallelogram consists of Link 5, Link 6, Link 4 and Link 7 and the nature of the parallelogram makes $r_6 = r_7$. By the definition of a parallelogram, Link 4 and Link 5 remain horizontal all the time. Thus, there is no rotation of the slider link. When $r_6 = r_8$, θ_{18} and θ_{16} would move nearly equal. Virtual work method results would prove it.

To fully understand the motion of the mechanism, in another word to complete kinematic analysis of the mechanism locations of the all points should be identified for any input. Since the mechanism has 2 DOF, all point locations can be calculated with 2 inputs.

After creating functions for positions of points, preliminaries would be decided for our desired motion.

Firstly, choose θ_{18} and θ_{16} as input and derive equations for all other points. Position of P6 is known. Position of P8 is

$$X_{P_8} = X_{P_6} + r_8 \cos \theta_{18} \quad 4-5$$

$$Y_{P_8} = Y_{P_6} + r_8 \sin \theta_{18} \quad 4-6$$

Similarly, the positions of P9, P10, P11, P4, P5 and P3 are calculated, respectively as

$$X_{P_9} = X_{P_8} + r_{51} \quad 4-7$$

$$Y_{P_9} = Y_{P_8} \quad 4-8$$

$$X_{P_{10}} = X_{P_9} + r_{52} \quad 4-9$$

$$Y_{P_{10}} = Y_{P_9} \quad 4-10$$

$$X_{P_{11}} = X_{P_{10}} + r_{53} \quad 4-11$$

$$Y_{P_{11}} = Y_{P_{10}} \quad 4-12$$

$$X_{P_4} = X_{P_9} + r_6 \cos \theta_{16} \quad 4-13$$

$$Y_{P_4} = Y_{P_9} - r_6 \sin \theta_{16} \quad 4-14$$

$$X_{P_5} = X_{P_4} + r_{42} \quad 4-15$$

$$Y_{P_5} = Y_{P_4} \quad 4-16$$

$$X_{P_3} = X_{P_4} - r_{41} \quad 4-17$$

$$Y_{P_3} = Y_{P_4} \quad 4-18$$

With the equations above, the positions of all points except for P2 can be calculated. Using cosine theorem, the position of P2 can be formulated.

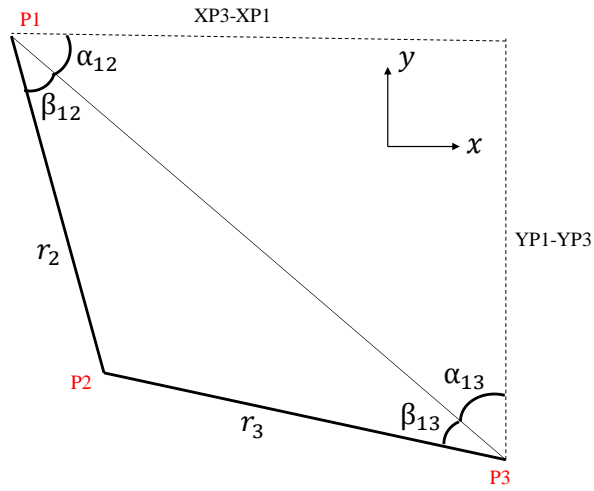


Figure 4.9. Position of Link 2 and Link 3

An arbitrary position of Link 2 and Link 3 are given in Figure 4.9. Then

$$\theta_{12} = \alpha_{12} + \beta_{12} \quad 4-19$$

where;

$$\alpha_{12} = \tan^{-1} \left(\frac{Y_{P_1} - Y_{P_3}}{X_{P_3} - X_{P_1}} \right) \quad 4-20$$

$$\beta_{12} = \cos^{-1} \left(\frac{r_2^2 + [(X_{P_1} - X_{P_3})^2 + (Y_{P_1} - Y_{P_3})^2] - r_3^2}{2r_2 \sqrt{(X_{P_1} - X_{P_3})^2 + (Y_{P_1} - Y_{P_3})^2}} \right) \quad 4-21$$

Angle of Link 2, θ_{12} , is calculated.

$$\theta_{13} = \alpha_{13} + \beta_{13} \quad 4-22$$

where;

$$\alpha_{13} = \tan^{-1}\left(\frac{X_{P_3} - X_{P_1}}{Y_{P_1} - Y_{P_3}}\right) \quad 4-23$$

$$\beta_{13} = \cos^{-1}\left(\frac{r_3^2 + [(X_{P_1} - X_{P_3})^2 + (Y_{P_1} - Y_{P_3})^2] - r_2^2}{2r_3\sqrt{(X_{P_1} - X_{P_3})^2 + (Y_{P_1} - Y_{P_3})^2}}\right) \quad 4-24$$

Angle of Link 3, θ_{13} is calculated. The kinematics of the mechanism is completely formulated in terms of θ_{16} and θ_{18} .

4.6 Dimensions of Proposed Mechanism

Proposed mechanism and its kinematic solution is shared in the previous section. Stroke and axis drift values of mechanism change with the dimensions. Dimensions of links can be applied to any scaled for application. To compare the stroke and axis drift values with the previous study, dimensions of the links are selected with the same as previous study of Tanik et al. [10]. Dimensions of mechanism is shown in Figure 4.10.

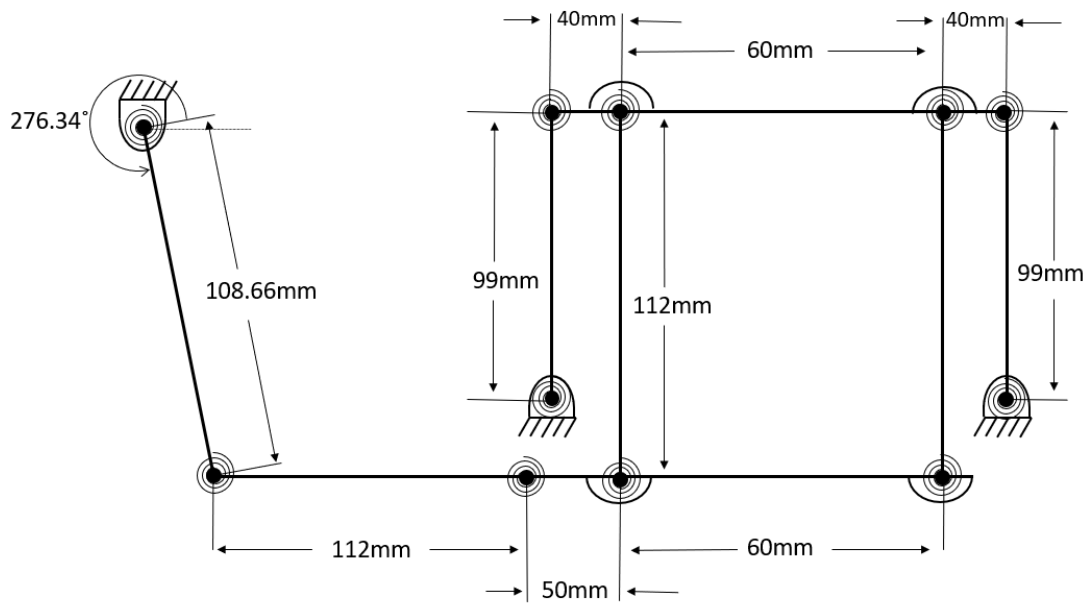


Figure 4.10. Dimensions of Proposed Mechanism

Dimensions of 3D model of proposed mechanism is given Appendix C.

4.7 Kinematic Simulation

Having formulated the kinematic analysis, a script is created at MATLAB. That script includes all calculations of the position of points and visualization of the mechanism. Since the mechanism has 2 degrees of freedom, θ_{16} and θ_{18} are assigned as an input.

Our aim is to catch desired angles (3° , 6° , 9° and 12°) of θ_{12} . For desired values of θ_{12} , stroke and axis drift of the system is calculated and tabulated in Table 4.2.

Figure 4.11 shows the initial state of the mechanism. For desired angles of θ_{12} , mechanism position is illustrated in Figures Figure 4.12-Figure 4.19.

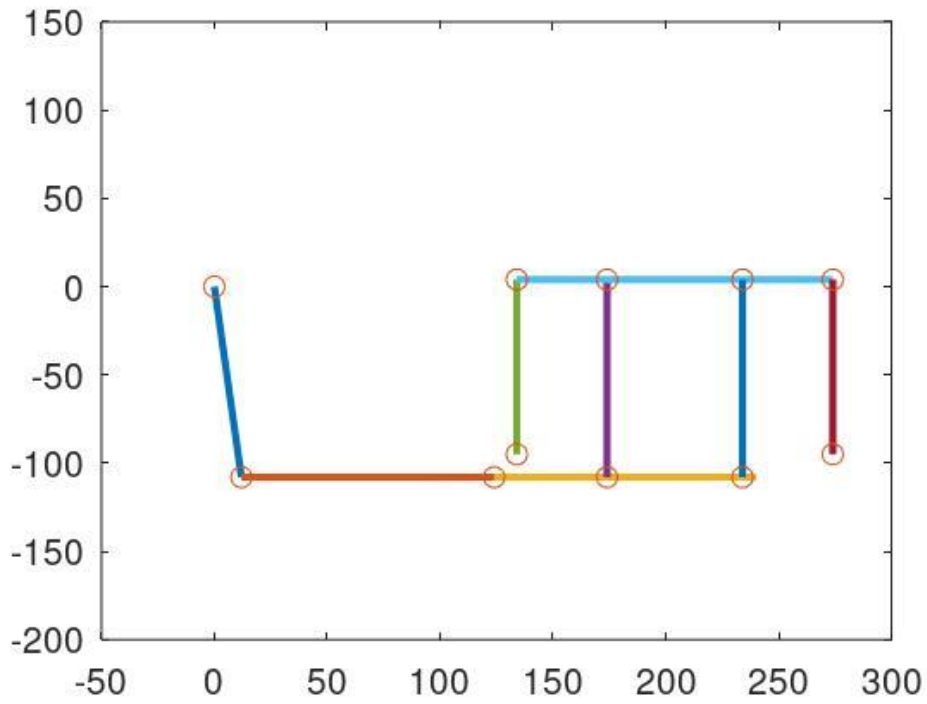


Figure 4.11. Results of kinematic analysis (Initial state)

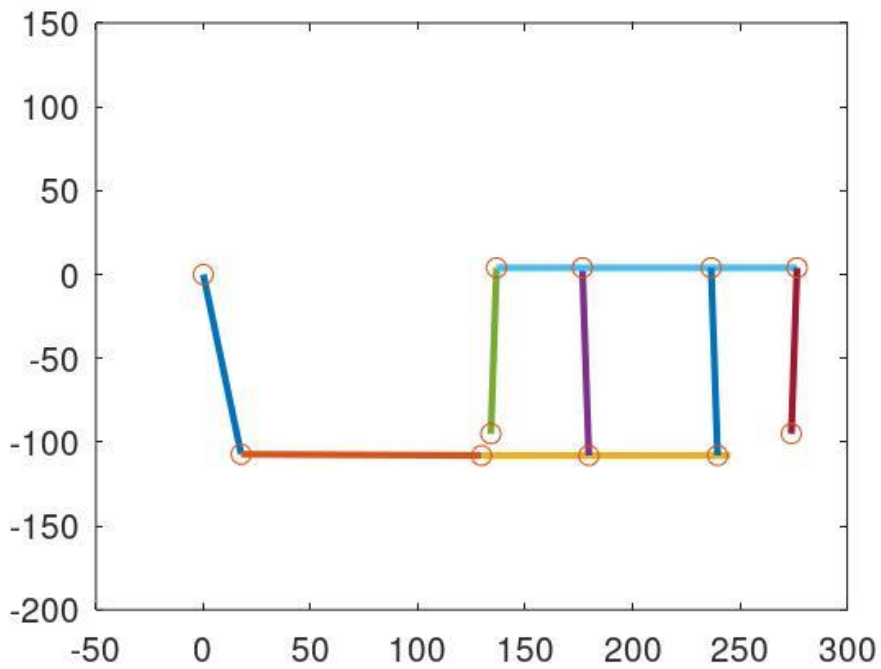


Figure 4.12. Results of kinematic analysis (3° CCW)

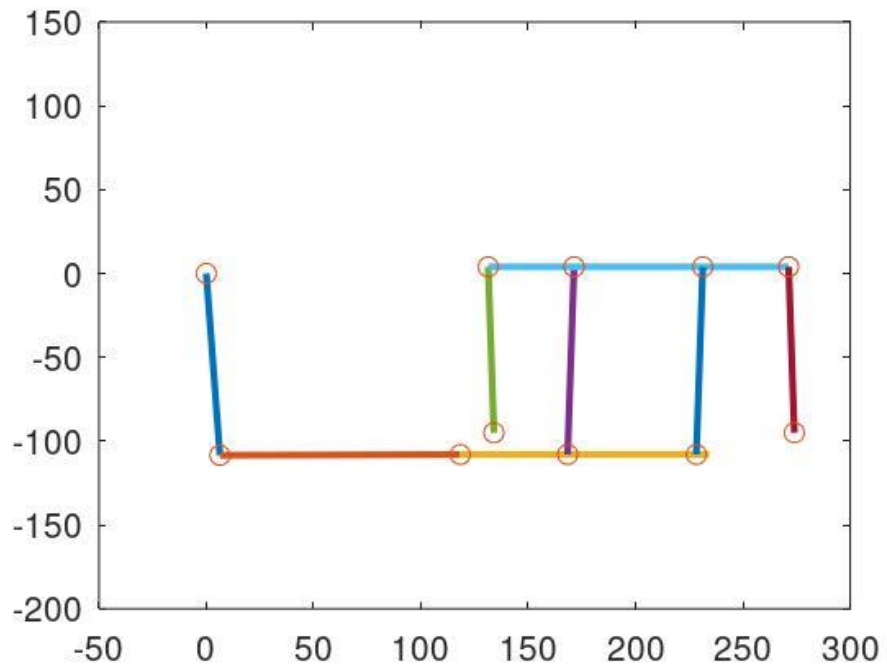


Figure 4.13. Results of kinematic analysis (3° CW)

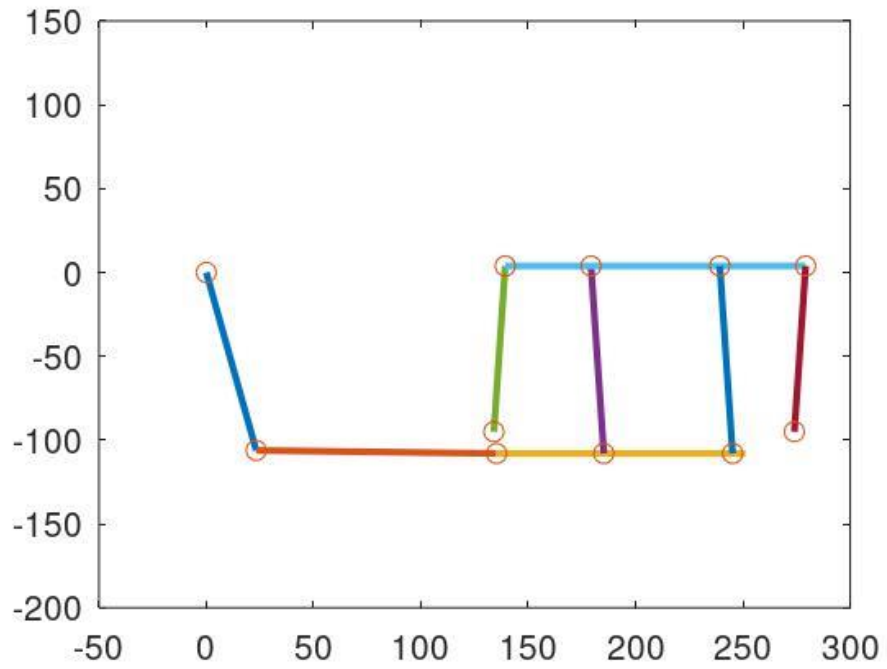


Figure 4.14. Results of kinematic analysis (6° CCW)

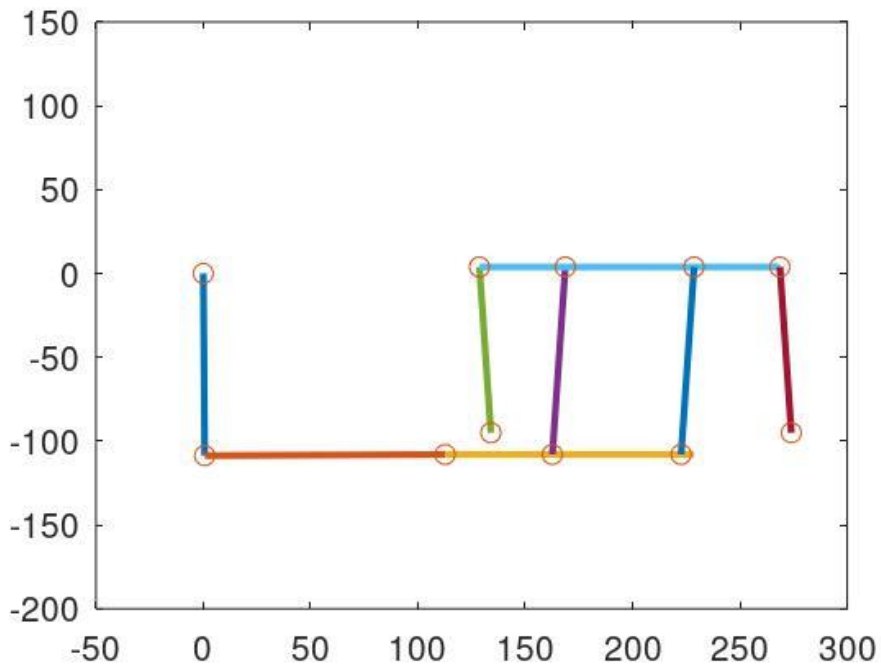


Figure 4.15. Results of kinematic analysis (6° CW)

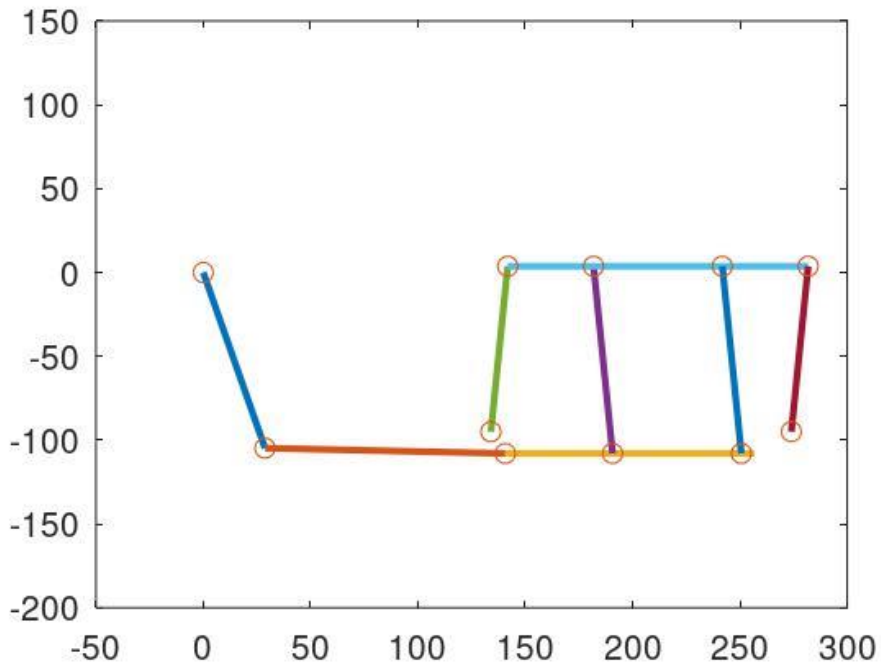


Figure 4.16. Results of kinematic analysis (9° CCW)

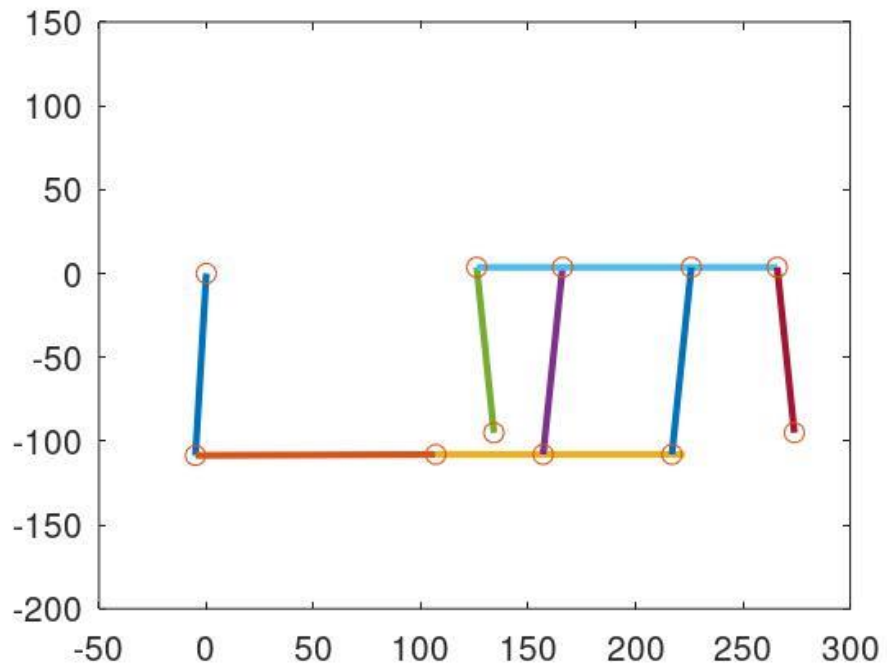


Figure 4.17. Results of kinematic analysis (9° CW)

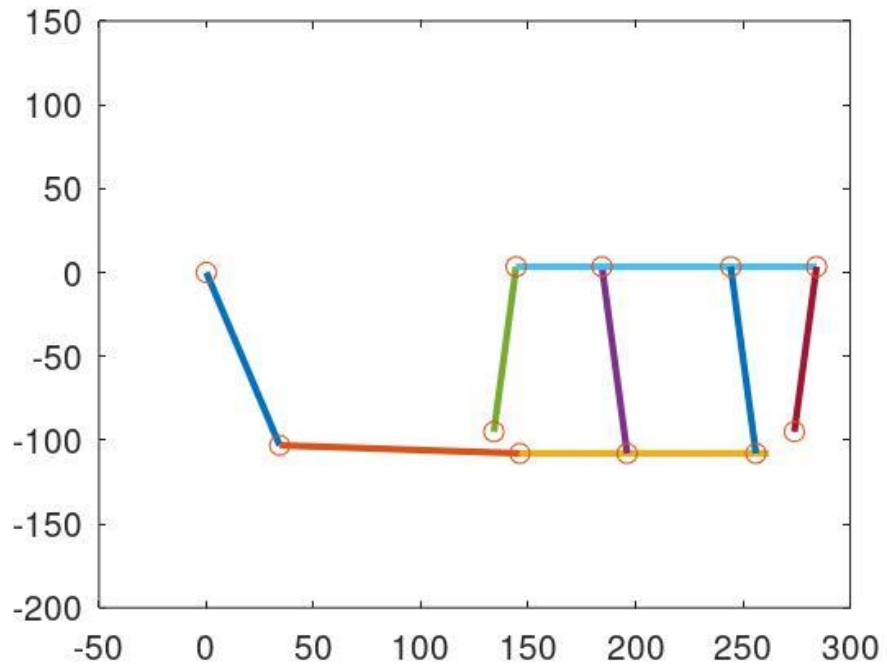


Figure 4.18. Results of kinematic analysis (12° CCW)

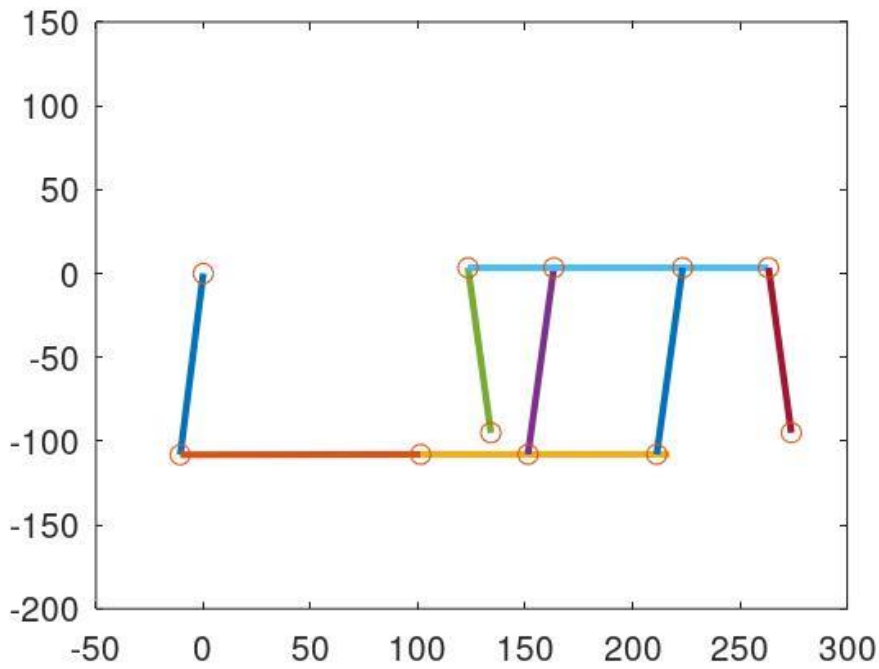


Figure 4.19. Results of kinematic analysis (12° CW)

Table 4.2 Kinematic Results of the Mechanism

Case	θ_{16} (°)	θ_{18} (°)	θ_{12} (°)	Stroke (mm)	Axis Drift (mm)
Initial	270	90	83.66	0	0
Case #1 (3° CCW)	271.53	88.47	80.66	5.65	4.65E-3
Case #2 (3° CW)	268.46	91.539	86.66	5.67	4.68E-3
Case #3 (6° CCW)	273.05	86.95	77.66	11.21	1.84E-2
Case #4 (6° CW)	266.92	93.08	89.66	11.352	1.88E-2
Case #5 (9° CCW)	274.54	85.46	74.66	16.71	4.11E-2
Case #6 (9° CW)	265.36	94.64	92.66	17.05	4.25E-2
Case #7 (12° CCW)	276.01	83.99	71.66	22.09	7.14E-2
Case #8 (12° CW)	263.82	96.18	95.66	22.72	7.55E-2

Table 4.2 indicates characteristic values of kinematic analysis results of mechanism. Inputs of kinematic analysis, θ_{16} and θ_{18} , must be equal to make axis drift of the mechanism minimized. With virtual work method solutions equal motion of θ_{16} and θ_{18} are provided. Lengths of Link 6 and Link 8 are affects the motion of θ_{16} and θ_{18} . When this criterion is provided, the slider link of the mechanism translates nearly only in a constant level (i.e. constant y coordinate).

Although inputs of kinematic analysis are θ_{16} and θ_{18} , the input of slider mechanism is the angle of the crank. For this reason, in the mechanism, when crank of the mechanism is driven θ_{16} and θ_{18} should change equally, or Link 6 and Link 8 should deform equally. This criterion can be employed with the help of the spring constant and link lengths of the mechanism. When the spring constant of a flexural hinge is increased, that hinge deforms less and reduces the motion of the link connected with that flexural hinge.

4.8 Virtual Work Method

Virtual work method is used to analyze proposed mechanism. Springs of mechanism are removed and torques due to these springs are calculated and virtual work on each spring is derived.

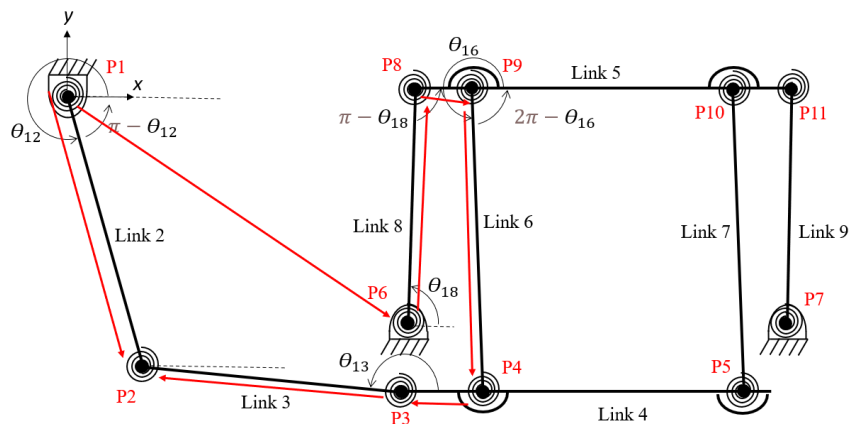


Figure 4.20. Loop of Virtual Work Method

A loop closure equation (LCE) is derived. The vector loops are presented in Figure 4.20.

$$r_2 * e^{i\theta_{12}} = X_{P_6} + iY_{P_6} + r_8 * e^{i\theta_{18}} + r_{51} + r_6 * e^{i\theta_{16}} - r_{41} + r_3 * e^{i\theta_{13}} \quad 4-25$$

Where X_{P_6} and Y_{P_6} are the position values of Point 6.

$$r_2 * \cos(\theta_{12}) = X_{P_6} + r_8 \cos(\theta_{18}) + r_{51} + r_6 \cos(\theta_{16}) - r_{41} + r_3 \cos(\theta_{13}) \quad 4-26$$

$$r_2 * \sin(\theta_{12}) = Y_{P_6} + r_8 \sin(\theta_{18}) + r_6 \sin(\theta_{16}) + r_3 \sin(\theta_{13}) \quad 4-27$$

Differentiating Eqs. 4-26 and 4-27 yields

$$\begin{aligned} r_2 \sin(\theta_{12}) \delta\theta_{12} &= r_8 \sin(\theta_{18}) \delta\theta_{18} + r_6 \sin(\theta_{16}) \delta\theta_{16} + r_3 \sin(\theta_{13}) \delta\theta_{13} \end{aligned} \quad 4-28$$

$$\begin{aligned} r_2 \cos(\theta_{12}) \delta\theta_{12} &= r_8 \cos(\theta_{18}) \delta\theta_{18} + r_6 \cos(\theta_{16}) \delta\theta_{16} + r_3 \cos(\theta_{13}) \delta\theta_{13} \end{aligned} \quad 4-29$$

Let θ_{12} and θ_{18} be the generalized coordinates. $\delta\theta_{13}$ and $\delta\theta_{16}$ can be derived from eqn. 4-28 and 4-29.

$$\delta\theta_{13} = \frac{-r_2\delta\theta_{12} \sin(\theta_{16} - \theta_{12}) - r_8\delta\theta_{18} \sin(\theta_{18} - \theta_{16})}{r_3 \sin(\theta_{13} - \theta_{16})} \quad 4-30$$

$$\delta\theta_{16} = \frac{r_2\delta\theta_{12} \sin(\theta_{13} - \theta_{12}) + r_8\delta\theta_{18} \sin(\theta_{18} - \theta_{13})}{r_6 \sin(\theta_{13} - \theta_{16})} \quad 4-31$$

Before deriving the virtual work formulas, initial positions of θ_{12} , θ_{13} , θ_{16} and θ_{18} are assigned.

$$\theta_{12_0} = 1.535\pi, \theta_{13_0} = \pi, \theta_{23_0} = 0.535\pi, \theta_{16_0} = \frac{3\pi}{2}, \theta_{18_0} = \frac{\pi}{2}, \theta_{64_0} = \frac{\pi}{2},$$

$$\theta_{85_0} = \frac{\pi}{2} \text{ and } \theta_{56_0} = \frac{\pi}{2}$$

Then, virtual work of active force and all springs (Figure 4.20) are;

$$\delta W_1 = -k (\theta_{12} - \theta_{12_0}) \delta\theta_{12} \quad 4-32$$

$$\delta W_2 = -k (\theta_{23} - \theta_{23_0}) \delta\theta_{23} \quad 4-33$$

where $\theta_{23} = \theta_{12} - \theta_{13}$ and $\delta\theta_{23} = \delta\theta_{12} - \delta\theta_{13}$.

$$\delta W_3 = -k (\theta_{13} - \theta_{13_0}) \delta\theta_{13} \quad 4-34$$

$$\delta W_4 = -k (\theta_{64} - \theta_{64_0}) \delta\theta_{64} \quad 4-35$$

where $\theta_{64} = \theta_{16} - \pi$ and $\delta\theta_{64} = \delta\theta_{16}$.

$$\delta W_5 = \delta W_4 \quad 4-36$$

$$\delta W_6 = -k (\theta_{18} - \theta_{18_0}) \delta\theta_{18} \quad 4-37$$

$$\delta W_7 = \delta W_6 \quad 4-38$$

$$\delta W_8 = -k (\theta_{85} - \theta_{85_0}) \delta\theta_{85} \quad 4-39$$

where $\theta_{85} = \pi - \theta_{18}$ and $\delta\theta_{85} = -\delta\theta_{18}$.

$$\delta W_9 = \delta W_8 \quad 4-40$$

$$\delta W_{10} = -k (\theta_{56} - \theta_{56_0}) \delta\theta_{56} \quad 4-41$$

where $\theta_{56} = 2\pi - \theta_{16}$ and $\delta\theta_{56} = -\delta\theta_{16}$.

$$\delta W_{11} = \delta W_{10} \quad 4-42$$

$$\delta W_e = T_e \delta\theta_{12} \quad 4-43$$

where T_e is external input torque.

Then the virtual work of all the active forces is given by

$$\begin{aligned} \delta W = & \delta W_1 + \delta W_2 + \delta W_3 + \delta W_4 + \delta W_5 + \delta W_6 + \delta W_7 + \delta W_8 \\ & + \delta W_9 + \delta W_{10} + \delta W_{11} + \delta W_e \end{aligned} \quad 4-44$$

Substituting Eqs. 4-30 and 4-31 into Eq. 4-44 yields

$$\delta W = \delta\theta_{12}Q_1 + \delta\theta_{18}Q_2 \quad 4-45$$

According to principle of virtual work, a necessary and sufficient condition is that Q_1 and Q_2 must vanish:

$$Q_1 = 0, Q_2 = 0.$$

So, two equilibrium equations can be can be obtained as:

$$\begin{aligned} & (-r_6\theta_{12_0}r_2 \sin(\theta_{12} - \theta_{16}) + 2Ar_3r_6\theta_{12_0} - r_6\pi Ar_3 \\ & \quad + r_6\theta_{13}Ar_3 + 4r_3\theta_{16}r_2 \sin(\theta_{12} - \theta_{13}) \\ & \quad + r_6\theta_{12}r_2 \sin(\theta_{12} - \theta_{16}) \\ & \quad - 6r_3\pi r_2 \sin(\theta_{12} - \theta_{13}) - 2Ar_3r_6\theta_{12})k \\ & = -Ar_3r_6T_e \end{aligned} \quad 4-46$$

where $A = \sin(\theta_{13} - \theta_{16})$.

$$\begin{aligned}
& r_6 \theta_{12_0} r_8 \sin(\theta_{18} - \theta_{16}) - r_6 \theta_{12} r_8 \sin(\theta_{18} - \theta_{16}) \\
& + 2r_6 \pi \sin(\theta_{13} - \theta_{16}) r_3 \\
& - 4r_3 \theta_{16} r_8 \sin(\theta_{18} - \theta_{13}) \\
& - 4 \sin(\theta_{13} - \theta_{16}) r_3 \theta_{18} r_6 \\
& + 6r_3 \pi r_8 \sin(\theta_{18} - \theta_{13}) = 0
\end{aligned} \tag{4-47}$$

Then solving Eqs. 4-26, 4-27, 4-46 and 4-47 numerically, positions and angles of all links are calculated with input of T_e .

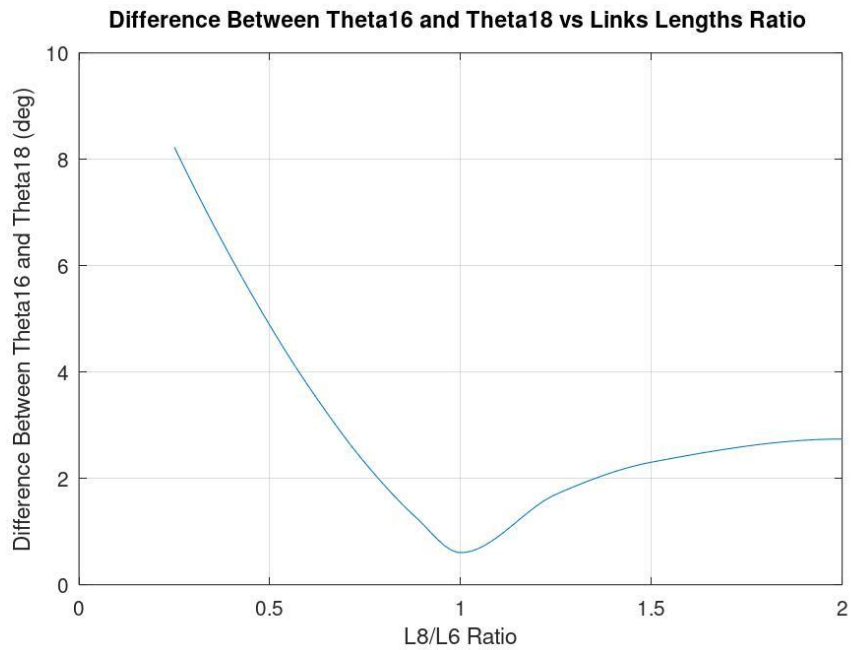


Figure 4.21. Difference Between θ_{16} and θ_{18} vs Links Lengths Ratio

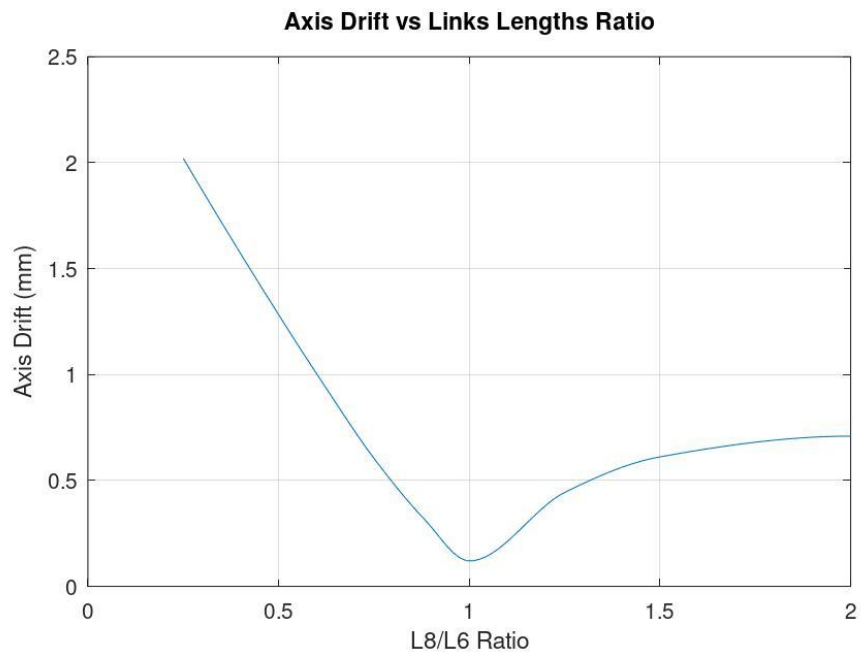


Figure 4.22. Axis Drift vs Links Lengths Ratio

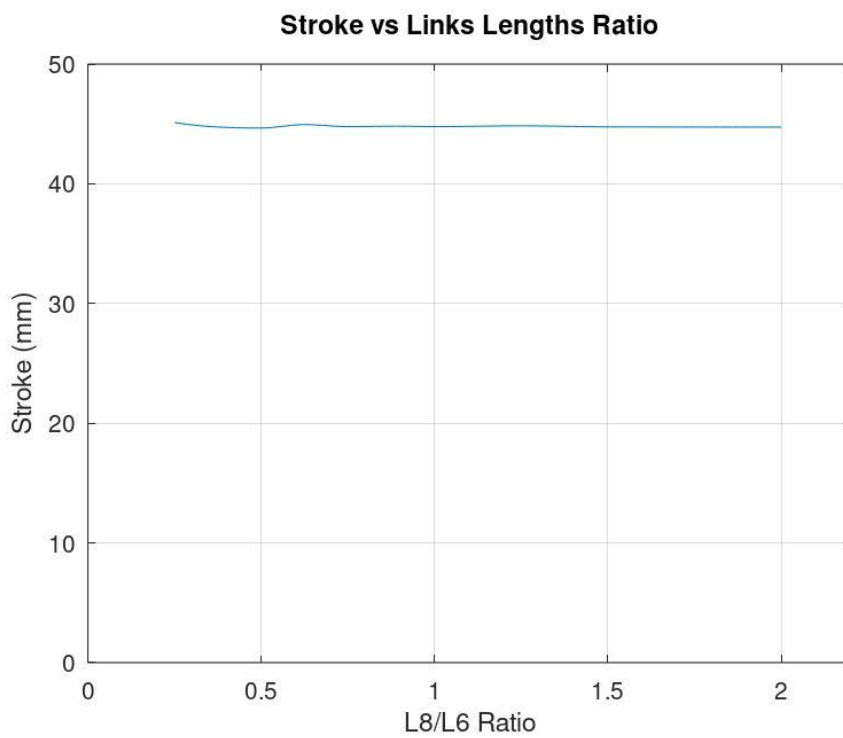


Figure 4.23. Stroke vs Links Lengths Ratio

In previous section, it is shown that θ_{16} and θ_{18} must be equal. Figure 4.21 shows the difference between θ_{16} and θ_{18} for different ratios of lengths. Difference between θ_{16} and θ_{18} and axis drift of output link is minimized when lengths of Link 8 and Link 6 are equal. Since main focus of this study is minimizing axis drift, the case of lengths of Link 8 and Link 6 are same would be the preferred one. But when the lengths are same, there would be some problems about 3D modelling and manufacturing the mechanism. Making lengths of Link 8 and Link 6 may be possible if Link 5 is not a straight element, but looks like a trapezoid. Bu this change affects the LCE and virtual work method equations.

3D model of proposed mechanism is created to make lengths of Link 8 and Link 6 closer to each other.

Ratio of lengths of Link 8 and Link 6 is 0.8839 for the proposed model of the mechanism. For this case maximum difference between θ_{16} and θ_{18} is 1.26° . For this case axis drift value is 0.3134 mm for 44.81 mm of stroke.

Figure 4.22 shows the axis drift values for different ratios of lengths of Link 8 and Link 6. Figure 4.23 shows the stroke values for different ratios of lengths of Link 8 and Link 6.

CHAPTER 5

FINITE ELEMENTS ANALYSES AND RESULTS

5.1 Analysis with 1D Elements

After the design steps are completed, the FEA model is created with 1D elements. According to the results of this analysis, the mechanism is updated. The advantage of using 1D elements in the models is that the model can be edited in the FEA software and runtime of the analysis is much shorter.

1D beam elements are used to simulate rigid link and 1D bush elements are used to simulate flexural hinges. To simulate flexural hinges, a coordinate system at the center of hinge is created and spring constant of that hinge is specified based on that coordinate system. Spring constants of T1, T2, T3, R1 and R2 coordinates are defined as $1\text{E}+10\text{ N}\cdot\text{mm}/\text{rad}$, which utilizes no motion in that direction. Stiffness of flexural hinge assigned to spring constant of R3 coordinate is $488\text{ N}\cdot\text{mm}/\text{rad}$ for all springs. With the selected properties of hinges, mechanism works in desired characteristic.

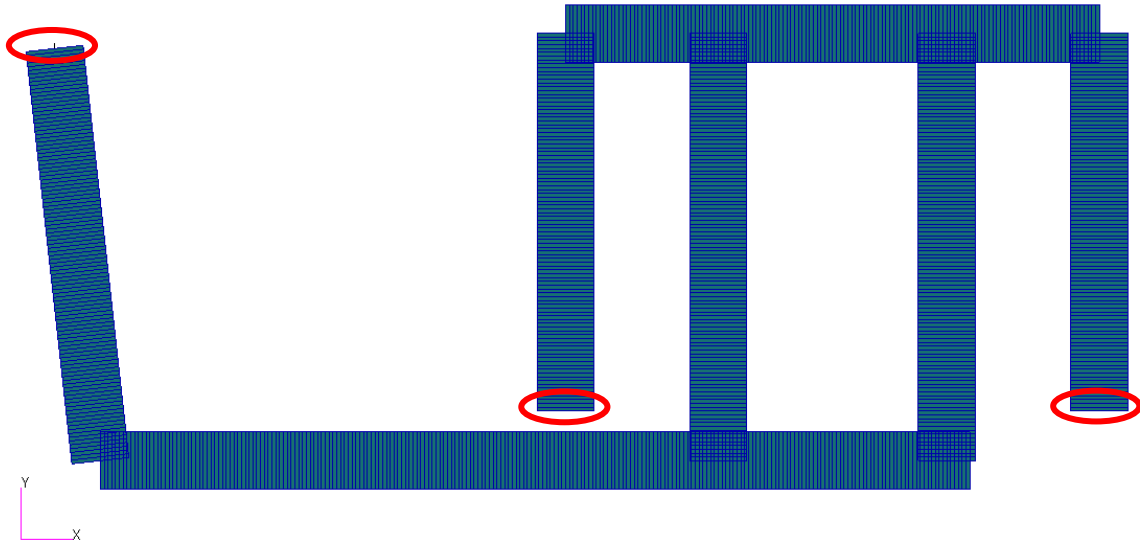


Figure 5.1. Representation of Elements and Boundary Conditions

For rigid links, elements with 1 mm lengths are created. Fix boundary conditions are applied to grounded faces that are encircled in Figure 5.1. Configurations for various crank angles are created. 3° , 6° , 9° and 12° of rotation in CW and in CCW directions are applied to the crank link.

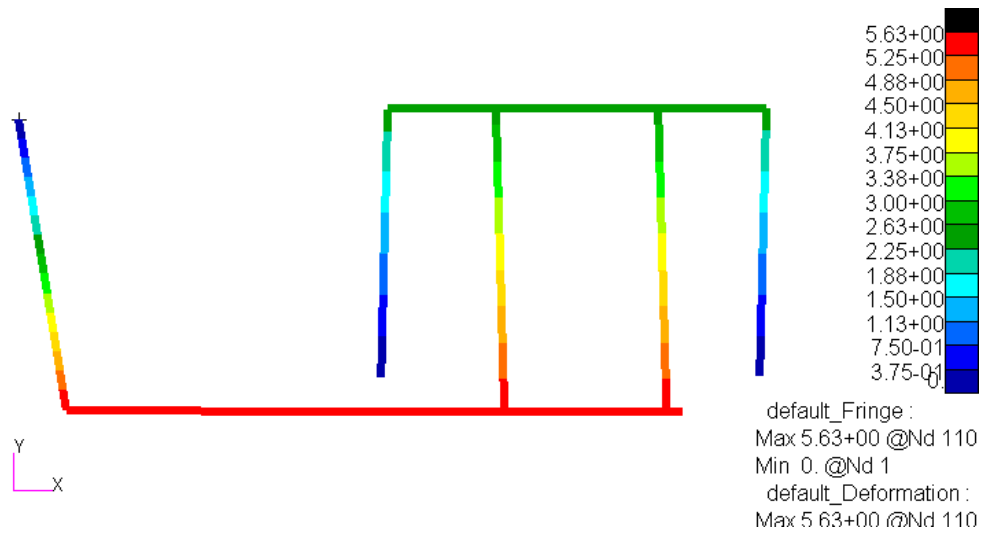


Figure 5.2. Results of stroke analysis with 1D elements (3° right)

Figure 5.2 shows the displacement result for 3° in CCW rotation case. Average output at the slider link is 5.59 mm and axis drift is 0.003 mm.

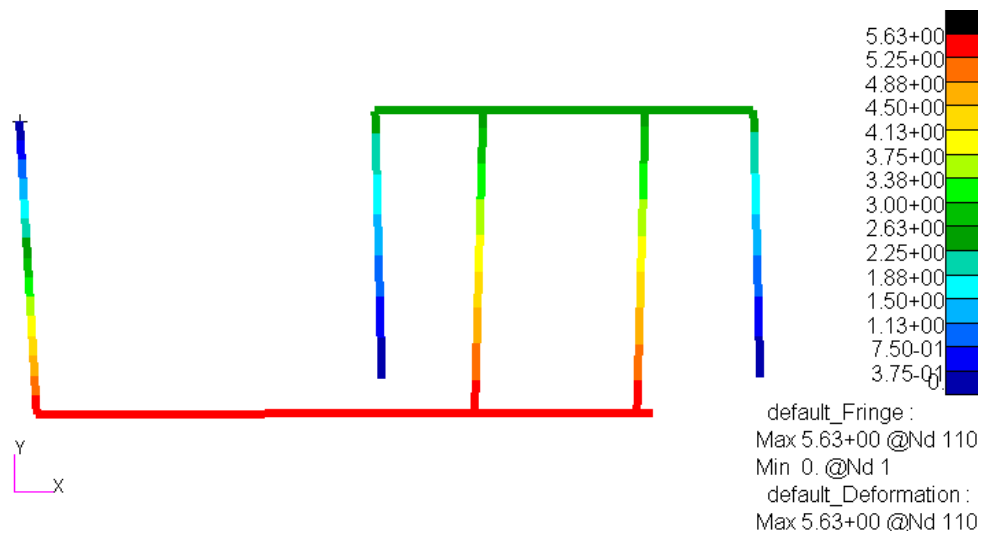


Figure 5.3. Results of stroke analysis with 1D elements (3° left)

Figure 5.3 shows the displacement result for 3° in CW rotation case. Average output at the slider link is 5.59 mm and axis drift is 0.003 mm.

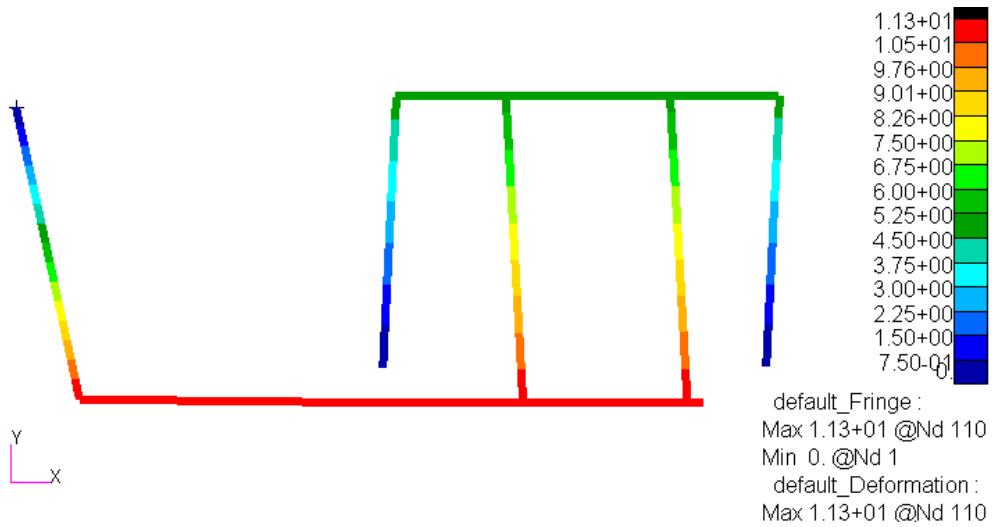


Figure 5.4. Results of stroke analysis with 1D elements (6° right)

Figure 5.4 shows the displacement result for 6° in CCW rotation case. Average output at the slider link is 11.19 mm and axis drift is 0.006 mm.

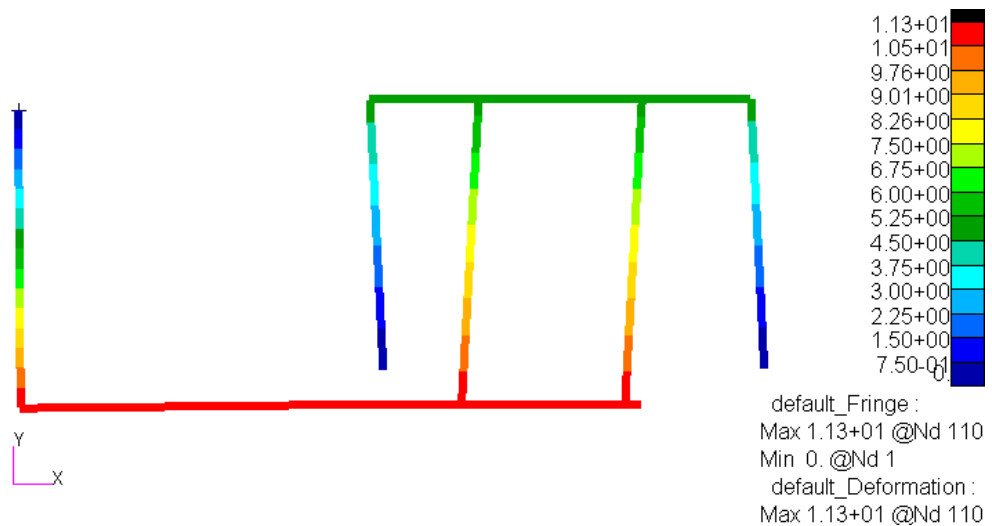


Figure 5.5. Results of stroke analysis with 1D elements (6° left)

Figure 5.5 shows the displacement result for 6° in CW rotation case. Average output at the slider link is 11.19 mm and axis drift is 0.006 mm.

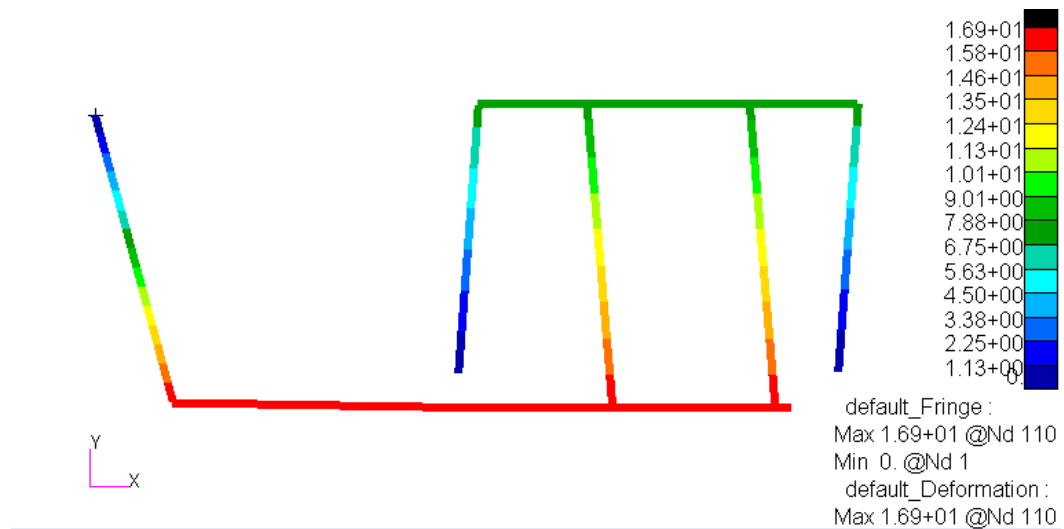


Figure 5.6. Results of stroke analysis with 1D elements (9° right)

Figure 5.6 shows the displacement result for 9° in CCW rotation case. Average output at the slider link is 16.78 mm and axis drift is 0.009 mm.

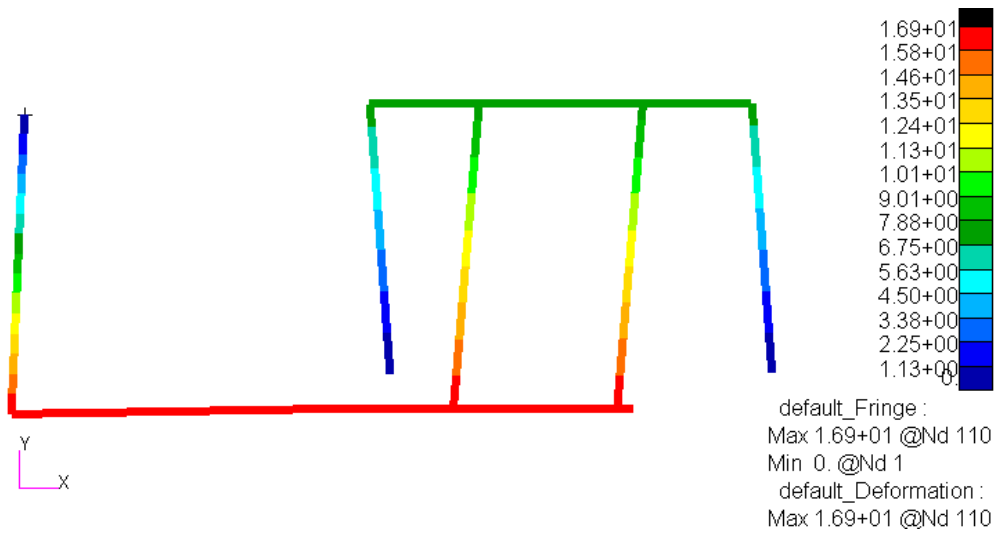


Figure 5.7. Results of stroke analysis with 1D elements (9° left)

Figure 5.7 shows the displacement result for 9° in CW rotation case. Average output at the slider link is 16.78 mm and axis drift is 0.009 mm.

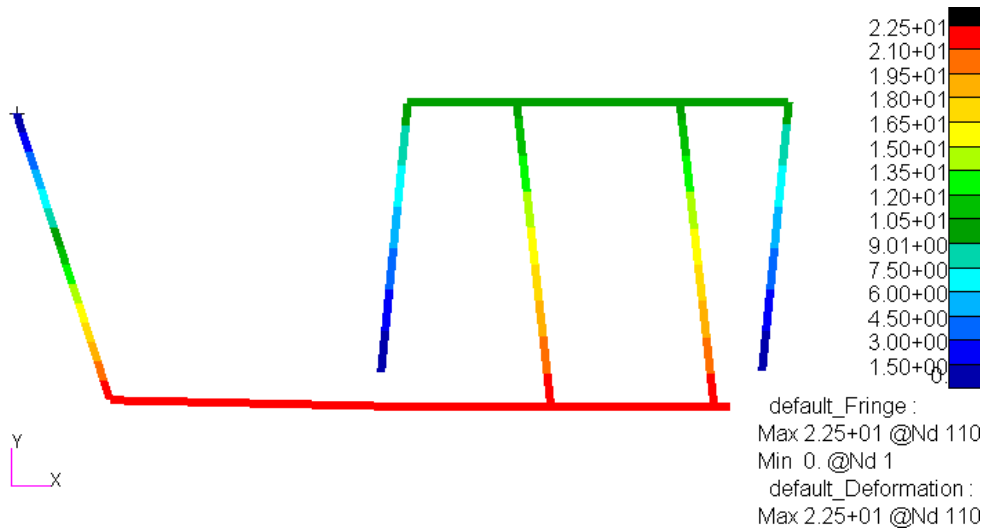


Figure 5.8. Results of stroke analysis with 1D elements (12° right)

Figure 5.8 shows the displacement result for 12° in CCW rotation case. Average output at the slider link is 22.38 mm and axis drift is 0.012 mm.

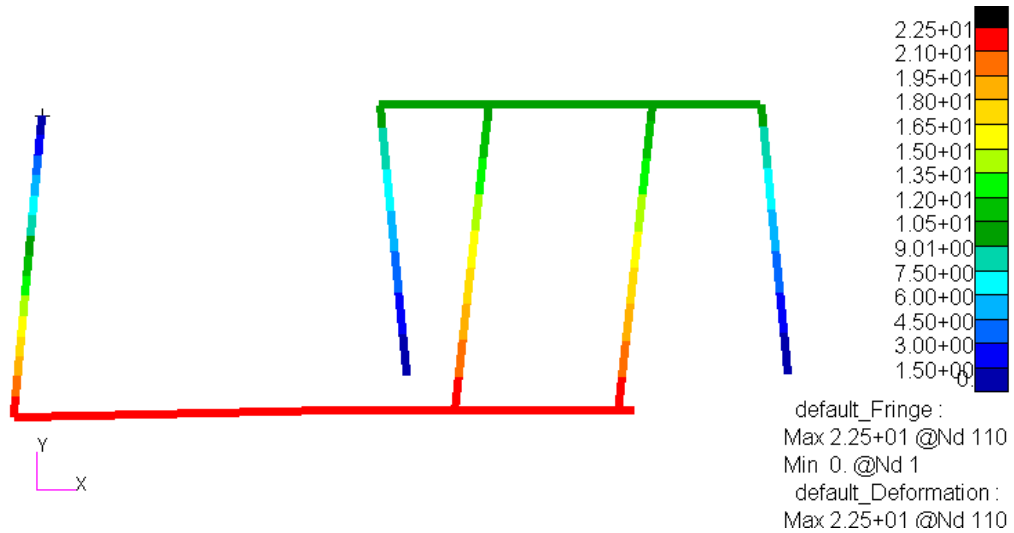


Figure 5.9. Results of stroke analysis with 1D elements (12° left)

Figure 5.8 shows the displacement result for 12° in CW rotation case. Average output at the slider link is 22.38 mm and axis drift is 0.012 mm.

Table 5.1 Results of FEA with 1D Elements

Analysis Case	Stroke (mm)	Axis Drift (mm)	Axis Rotation (°)
Case #1 (3° CCW)	5.59	2.85E-3	1.46E-03
Case #2 (3° CW)	5.59	2.85E-3	1.46E-03
Case #3 (6° CCW)	11.19	5.70E-3	2.92E-03
Case #4 (6° CW)	11.19	5.70E-3	2.92E-03
Case #5 (9° CCW)	16.78	8.55E-3	4.14E-03
Case #6 (9° CW)	16.78	8.55E-3	4.14E-03
Case #7 (12° CCW)	22.38	1.14E-2	5.52E-03
Case #8 (12° CW)	22.38	1.14E-2	5.52E-03

FEA is conducted for 8 cases of rotation of crank link. Results of analysis are tabulated at Table 5.1. Results of FEA with 1D elements mostly agreed with the analytical solution.

5.2 Analysis with 3D Elements

Analysis with 1D elements shows general motion and characteristics of the mechanism. Because of the element types of mechanism nonlinear effect of flexural hinges and links are not included in the analysis that was performed with 1D elements. That is why an FEA with 3D elements is required. The flow chart of analysis is shown in Figure 5.10.

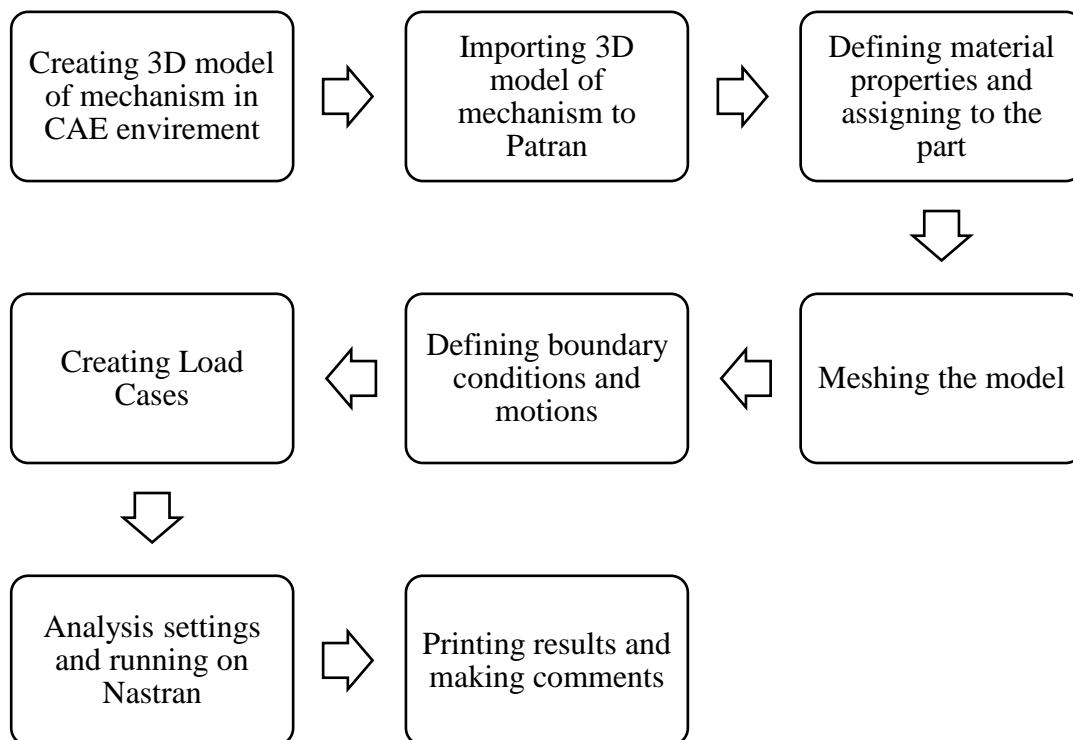


Figure 5.10. Analysis flow chart

5.2.1 Analysis Details

After creating 3D model of the mechanism, this model is imported to Patran as a single part. As mentioned before, polypropylene material is defined. Material properties are presented in the Material Selection section (Section 3.4). A solid property is created with polypropylene, and that property is assigned to the mechanism. A boundary condition named fix is created and applied to grounded surfaces. Grounded surfaces are encircled in Figure 5.11. Part is meshed with Tet10 type elements. Tet10 is an element in the shape of a tetrahedron with ten nodes. A displacement is applied to crank link to get a rotations for loadcases. 8 load cases are created with 8 rotation values of crank; 3° CCW, 3° CW, 6° CCW, 6° CW, 9° CCW, 9° CW, 12° CCW and 12° CW. Property assignment, meshing, boundary conditions and load cases are completed. Nonlinear analysis is selected and large displacement is activated. Large displacement feature updates stiffness matrix of mechanism after every iteration of analysis.

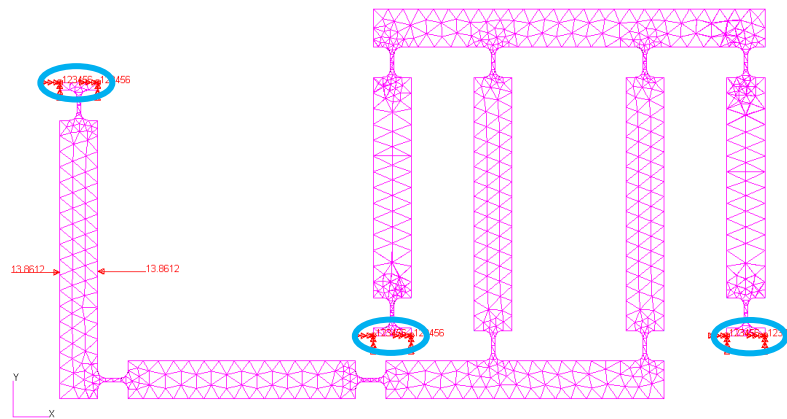


Figure 5.11. Mesh and Boundary Conditions of 3D Model

5.2.2 Results

Eight results are obtained for eight load cases. Figure 5.12 - Figure 5.19 show results of the displacement magnitude of mechanism and deformation shape.

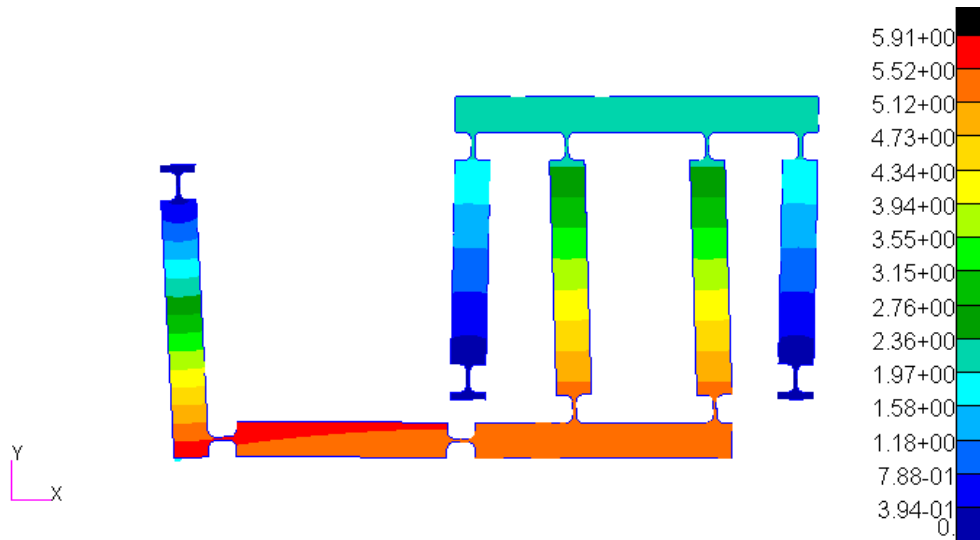


Figure 5.12. Results of stroke analysis with 3D elements (3° CCW) (mm)

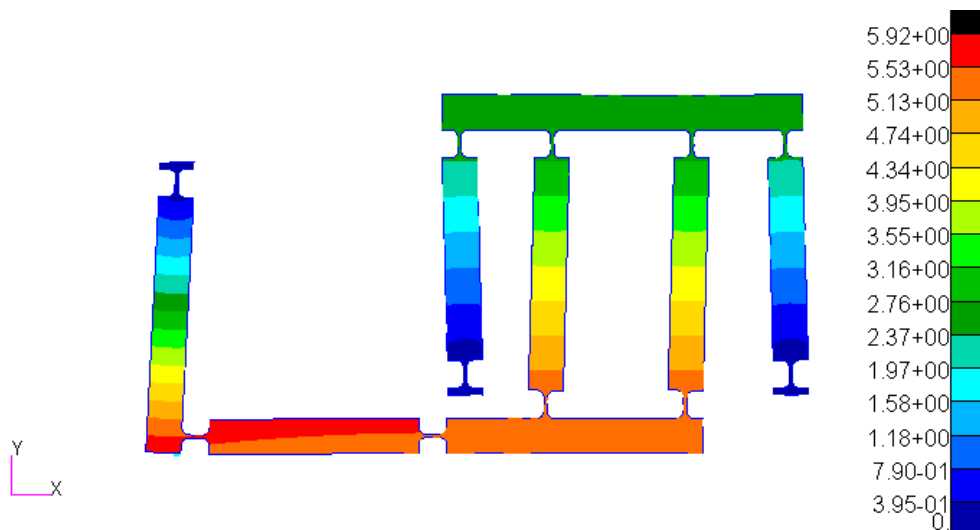


Figure 5.13. Results of stroke analysis with 3D elements (3° CW) (mm)

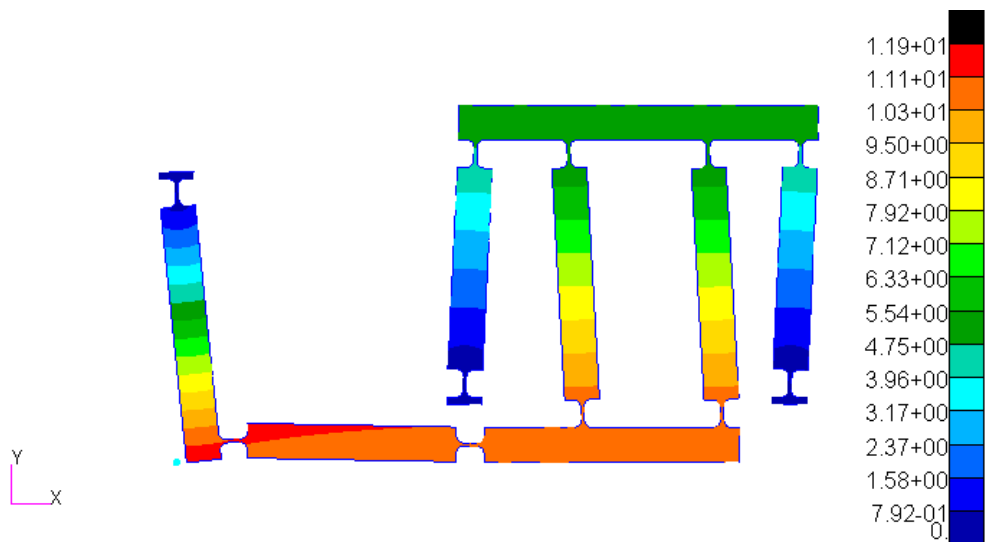


Figure 5.14. Results of stroke analysis with 3D elements (6° CCW) (mm)

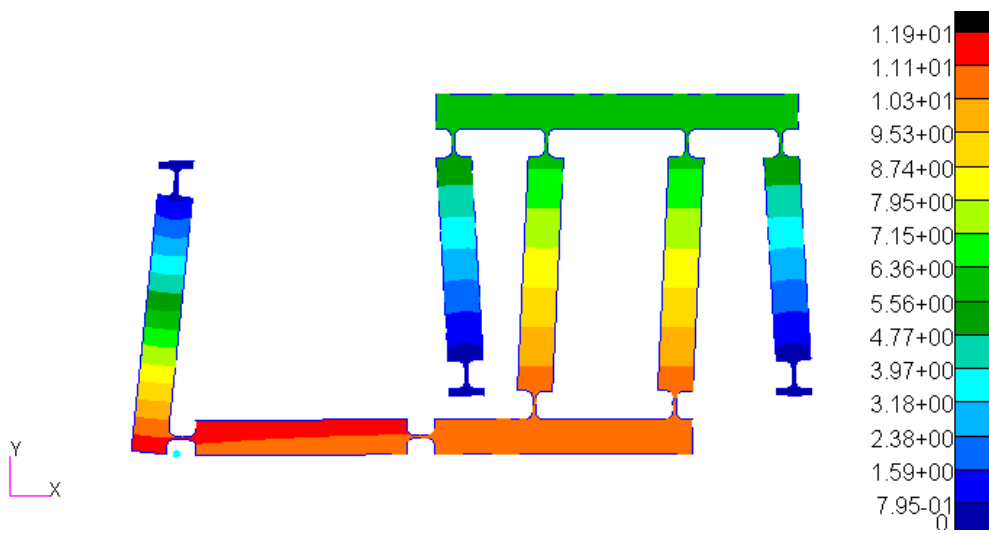


Figure 5.15. Results of stroke analysis with 3D elements (6° CW) (mm)

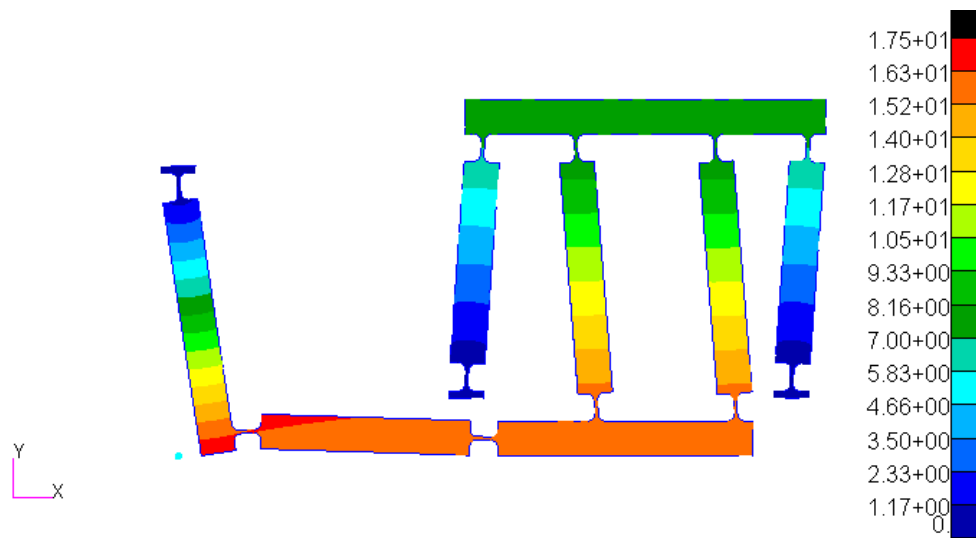


Figure 5.16. Results of stroke analysis with 3D elements (9° CCW) (mm)

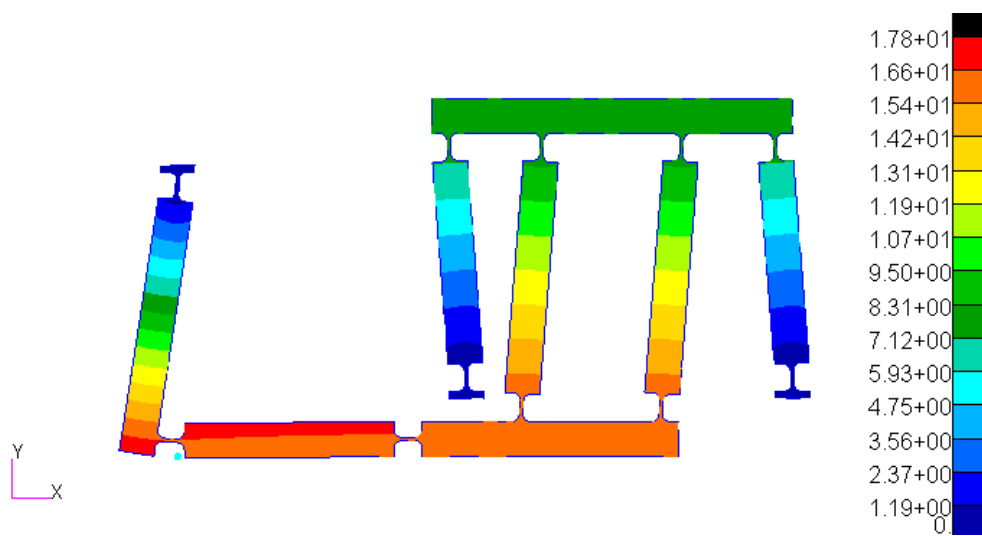


Figure 5.17. Results of stroke analysis with 3D elements (9° CW) (mm)

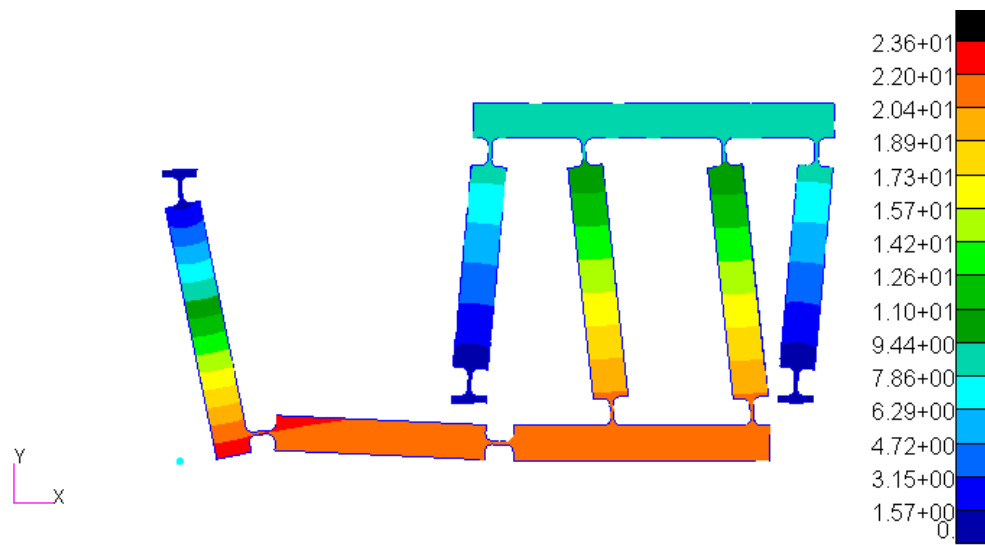


Figure 5.18. Results of stroke analysis with 3D elements (12° CCW) (mm)

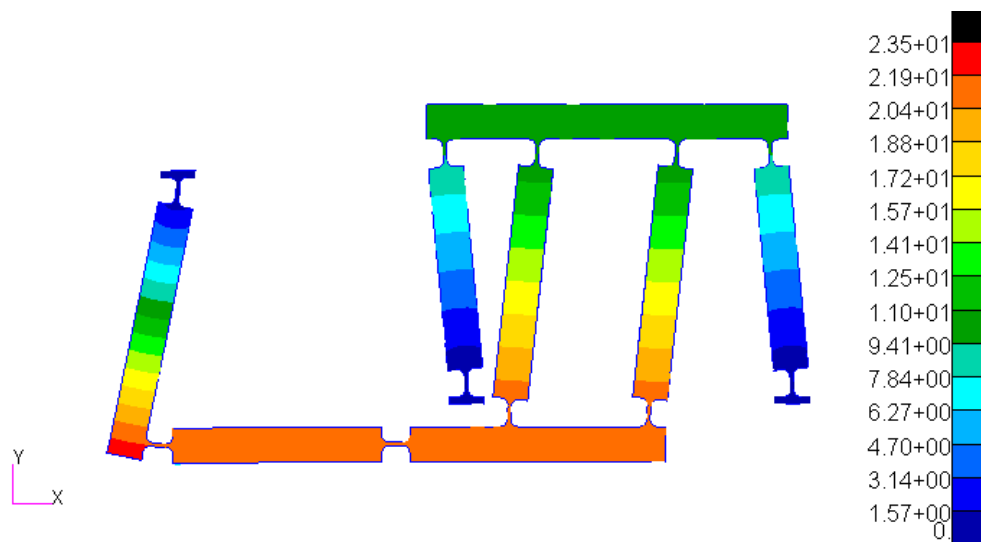


Figure 5.19. Results of stroke analysis with 3D elements (12° CW) (mm)

Stroke and axis drift values for every case is showed in Table 5.2.

Table 5.2 Results of FEA with 3D Elements

Analysis Case	<i>Stroke (mm)</i>	<i>Axis Drift (mm)</i>	<i>Axis Rotation (°)</i>
Case #1 (3° CCW)	5.60	1.98E-2	1.11E-03
Case #2 (3° CW)	5.65	1.28E-2	1.24E-03
Case #3 (6° CCW)	11.11	6.44E-2	5.89E-03
Case #4 (6° CW)	11.32	1.54E-2	2.52E-03
Case #5 (9° CCW)	16.59	1.71E-1	1.56E-03
Case #6 (9° CW)	16.97	5.98E-2	7.19E-03
Case #7 (12° CCW)	22.03	9.65E-2	2.68E-03
Case #8 (12° CW)	22.74	1.35E-1	1.28E-02

It is proven that, stroke of slider link achieved from 3D FEA are in agreement with results of analytical solution and FEA with 1D elements. Results also prove that PRBM derivation and application of mechanism is done correctly and properly.

CHAPTER 6

EXPERIMENTS

A physical prototype of a compliant slider-crank mechanism with proposed geometry and dimensions was manufactured and tested to verify theoretical analysis and FEA results.

6.1 Manufacturing Process

The manufacturing process of the mechanism is conducted using a 3-axis CNC machine. As presented in Chapter 5, the fully-compliant slider-crank mechanism is manufactured as a single piece. Three holes are added to stationary parts of the mechanism to fix it to the test board. The mechanism model for experiments is given in Figure 6.1. As mentioned Chapter 3.4 the mechanism is manufactured from a polypropylene plate of 15 mm thickness. The CoC (certificate of conformity) document of polypropylene which includes material properties is given Appendix A.

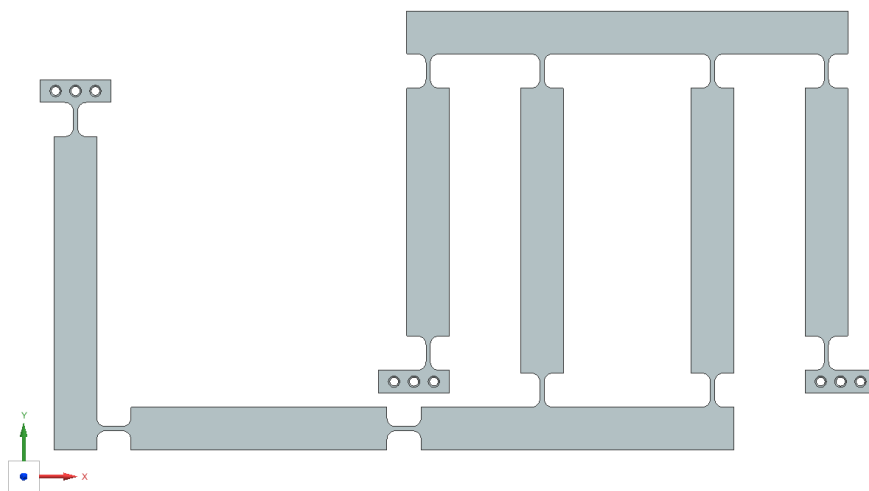


Figure 6.1. CAD model of mechanism for experiments.

6.2 Test Setup

After manufacturing the mechanism and other parts for experiment, the assembly process of test setup is started. The manufactured prototype of the mechanism is fixed to a metal plate. Stationary parts of the mechanism are connected to the plate by three M3 bolts and nuts. To deform the crank link in the desired range, two M6 bolts and two basic housing parts are also attached to the plate. Turning the bolt in the direction of desired motion deforms the crank link. By the way, the test setup to figure out and measure the motion of the mechanism is completed.

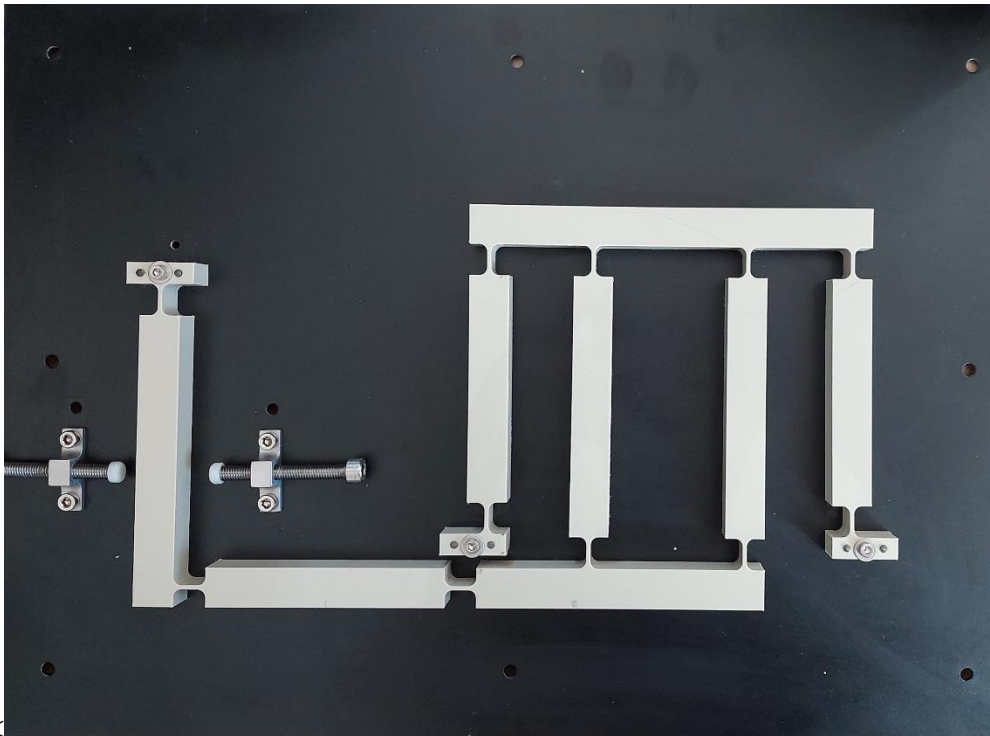


Figure 6.2. Test Setup

6.3 Test Results

The test setup is created to measure the motion of the mechanism. Stroke, axis drift and axis rotation of the slider link are measured for the specified rotation of the crank link. Since the actuation of the crank is made by bolt and depends on the precision of threads, the angle of rotation of the crank from the initial position is also measured.

Including the initial position, nine positions are measured using a coordinate measuring machine (CMM). Hexagon DEA Scirocco 102009 model CMM is used for measurements. This CMM has a precision of 0.001mm which is sufficient for the measurements. For every step, the positions of crank and slider link are measured. To measure the angle of the crank, 2 points from both right and left faces are measured and 2 lines are created. A midline is created from these lines, and measurements are derived from this midline. To measure stroke, axis drift and axis rotation of slider link, 4 lines are created by measure 2 points for each. From the midline of lines of right and left faces, stroke of mechanism is derived. The top and bottom faces' midline is used to derive axis drift and axis rotation. A view of the measurement program is given Appendix B.

The measurements are tabulated in Table 6.1.

Table 6.1 Measurement Results of Prototype for desired Angle of Crank

Analysis Case	Stroke (mm)	Axis Drift (mm)	Axis Rotation (°)
Case #1 (3° CCW)	5.85	8.11E-2	2.01E-3
Case #2 (3° CW)	5.88	5.12E-2	3.03E-3
Case #3 (6° CCW)	11.42	4.33E-2	6.96E-3
Case #4 (6° CW)	11.55	7.79E-2	12.08E-3
Case #5 (9° CCW)	16.99	1.51E-1	1.44E-3
Case #6 (9° CW)	17.38	1.92E-1	20.78E-3
Case #7 (12° CCW)	22.58	3.53E-1	4.32E-3
Case #8 (12° CW)	22.98	2.82E-1	33.09E-3

6.4 Comparison

Motion and characteristics of proposed motion is obtained in four ways; analytical solution, FEA with 1D elements, FEA with 3D elements and experimental results. The analytical solution is conducted by kinematic analysis and virtual work method and results are plotted using MATLAB. FEA analysis is established on MSC Patran/Nastran software. CMM is used to take measurements from the test setup of the prototype of proposed mechanism.

It is shown that the analytical solution, FEA with 1D elements and FEA with 3D elements results match with each other with very little error. So, comparing results of FEA with 3D elements and experiment is sufficient for this section. Stroke results of FEA and experiment are shared with Table 6.2 and Figure 6.3. The table also shows errors between these cases.

Table 6.2 Comparison of Stroke Values of mechanism

Analysis Case	<i>FEA with 3D Elements (mm)</i>	<i>Experiment (mm)</i>	<i>Error (mm)</i>
Case #1 (3° CCW)	5.60	5.85	0.25
Case #2 (3° CW)	5.65	5.88	0.23
Case #3 (6° CCW)	11.11	11.42	0.31
Case #4 (6° CW)	11.32	11.55	0.23
Case #5 (9° CCW)	16.59	16.99	0.4
Case #6 (9° CW)	16.97	17.38	0.41
Case #7 (12° CCW)	22.03	22.58	0.55
Case #8 (12° CW)	22.74	22.98	0.24

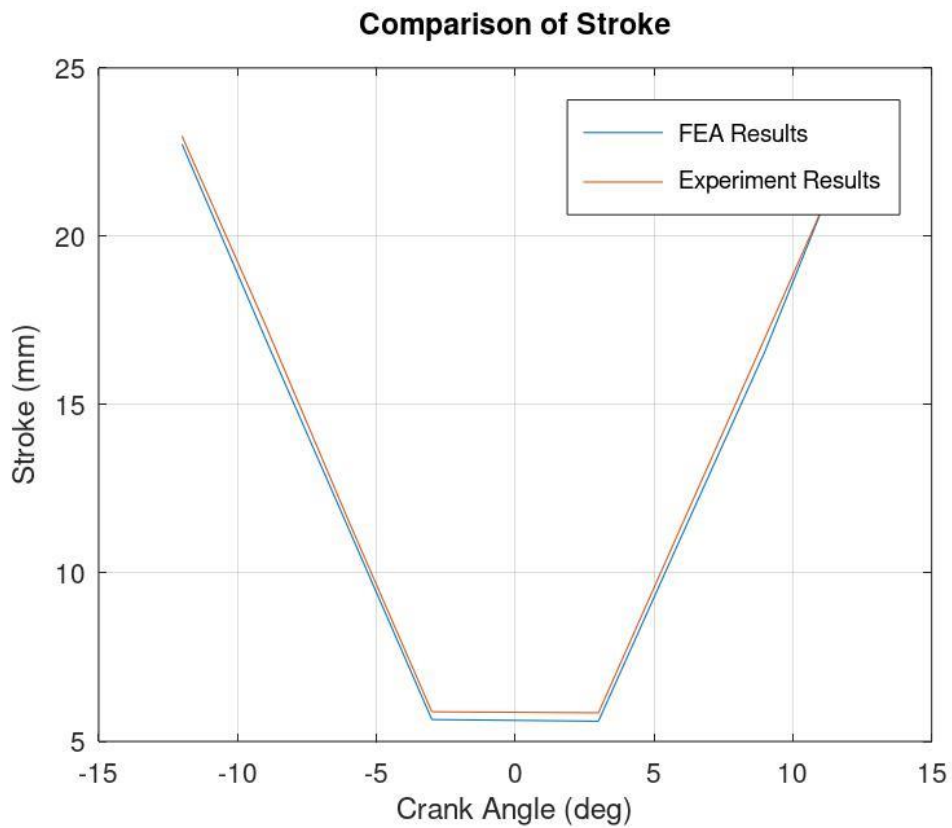


Figure 6.3. Comparison of Stroke Results of FEA and Experiment

The error between the results of FEA and the experiment is calculated. It is observed that the average error of stroke values is 0.33 mm. If this value is compared with the total stroke of the mechanism, the average percent error is 0.72%.

A comparison for axis drift is also needed. The initial centreline of the slider link is the datum axis of this link. Results of axis drift of mechanism from FEA and experiment are shared with Table 6.3 and Figure 6.4.

Table 6.3 Comparison of Axis Drift Values of mechanism

Analysis Case	<i>FEA with 3D</i>	<i>Experiment</i>	<i>Error (mm)</i>
	<i>Elements (mm)</i>	<i>(mm)</i>	
Case #1 (3° CCW)	1.98E-2	8.11E-2	6.13E-2
Case #2 (3° CW)	1.28E-2	5.12E-2	3.84E-2
Case #3 (6° CCW)	6.44E-2	4.33E-2	2.11E-2
Case #4 (6° CW)	1.54E-2	7.79E-2	6.25E-2
Case #5 (9° CCW)	1.71E-1	1.51E-1	2.00E-2
Case #6 (9° CW)	5.98E-2	1.92E-1	1.32E-1
Case #7 (12° CCW)	9.65E-2	3.53E-1	2.57E-1
Case #8 (12° CW)	1.35E-1	2.82E-1	1.47E-1

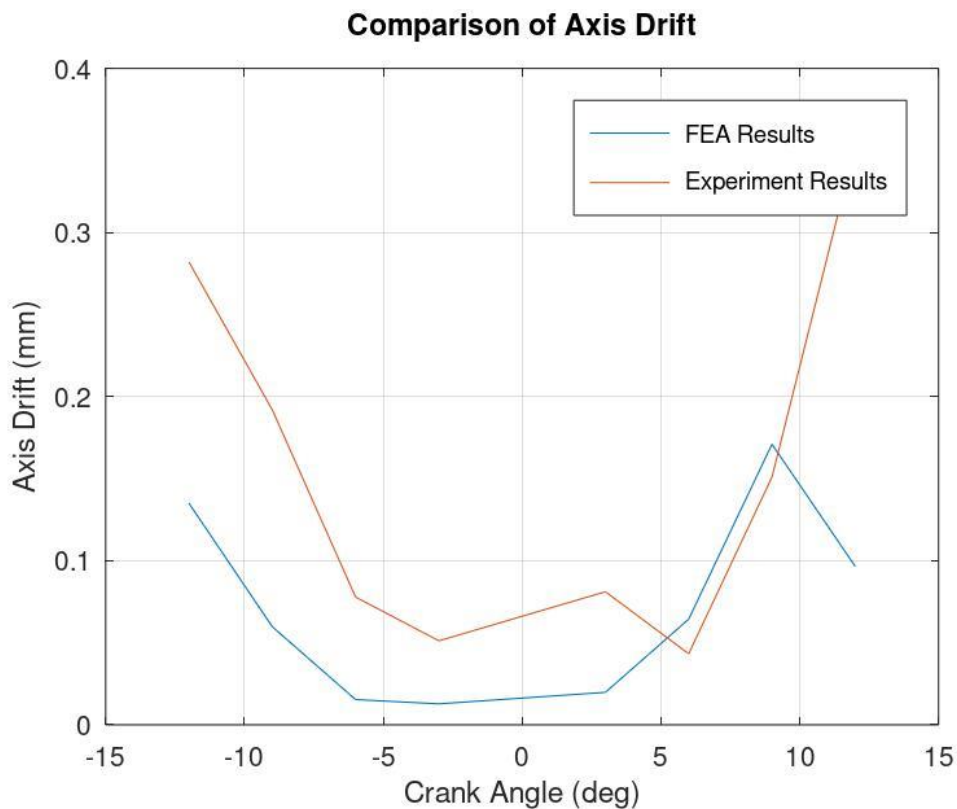


Figure 6.4. Comparison of Axis Drift Results of FEA and Experiment

Axis drift of mechanism is significantly small when compared to the stroke of the mechanism. The average absolute axis drift of the mechanism is 1.08E-1 mm for the motions with overall 45.56 mm stroke. The average error of axis drift between FEA results and experiment results is 9.24E-2 mm. Since axis drift values are in the order of one-tenth of a mm, measuring axis drift precisely is difficult, and error of measurement gets higher.

Axis rotation values from FEA and experiment are compared in Figure 6.5 and Table 6.4 Comparison of Axis Rotation Values of the Mechanism Table 6.4.

Table 6.4 Comparison of Axis Rotation Values of the Mechanism

Analysis Case	<i>FEA with 3D</i>		
	<i>Elements (°)</i>	<i>Experiment (°)</i>	<i>Error (°)</i>
Case #1 (3° CCW)	1.11E-3	2.01E-3	9.00E-4
Case #2 (3° CW)	1.24E-3	3.03E-3	1.79E-3
Case #3 (6° CCW)	5.89E-3	6.96E-3	1.07E-3
Case #4 (6° CW)	2.52E-3	12.08E-3	9.56E-3
Case #5 (9° CCW)	1.56E-3	1.44E-3	1.20E-4
Case #6 (9° CW)	7.19E-3	20.78E-3	1.36E-2
Case #7 (12° CCW)	2.68E-3	4.32E-3	1.64E-3
Case #8 (12° CW)	1.28E-2	33.09E-3	2.03E-2

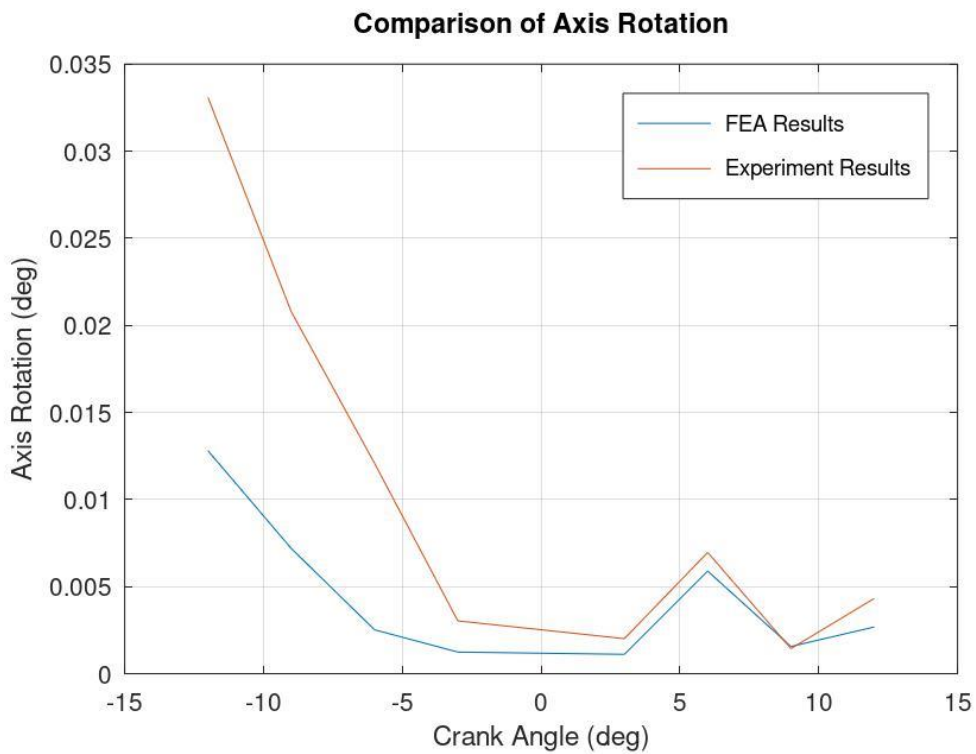


Figure 6.5. Comparison of Axis Rotation Results of FEA and Experiment

Axis rotation of mechanism is significantly small. So, measuring this much small dimensions gets big errors when compared to axis drift. Axis rotation values calculated by FEA and measured during the experiment are in the same order.

The design of compliant mechanisms always involves errors. The error between FEA and experiment is due to measurement errors. Since axis drift and axis rotation values are so small, errors become larger in percent. Lastly, experiment results fit with FEA results generally.

CHAPTER 7

CONCLUSIONS

The process of compliant mechanism design needs a versatile study to complete both structural and kinematic design of the mechanism. Rigid body replacement method is frequently used for design of compliant mechanisms. Analysing proposed mechanism is big part of design.

Slider-crank mechanism is a widely used mechanism that converts rotational motion of crank link to translational motion of slider link. In the literature, there are several studies about partially compliant mechanisms. Fully compliant slider-crank mechanism study is limited and mechanism of study has a remarkable axis drift which makes the mechanism unusable in the industry. Objective of the thesis is designing a slider-crank mechanism with minimized axis drift. A fully compliant slider-crank mechanism with minimized axis drift fulfills the capabilities of a rigid slider-crank mechanism.

Design procedure is started with the PRBM design and kinematic analysis until obtaining the desired motion. Then 3D model of the mechanism is created and the motion is observed with FEA. A manufactured prototype is tested and design procedure is validated with this step.

Hopefully, this fully compliant slider-crank mechanism with minimized axis drift would be used by engineers to fulfill the capabilities of a rigid mechanism.

As a future work, fatigue life of mechanism would be calculated and an experimental setup would be beneficial to validate calculations. Also, to improve performance of the mechanism, an underconstraint eliminator could be added to the double parallelogram part of the mechanism. To minimize the axis drift more lengths of Link 8 and Link 6 can be equalized by changing the geometric form of link 5.

Improving the performance of the mechanism and knowledge about concept would increase the use of mechanism in the industry.

REFERENCES

- [1] A. Midha, T. W. Norton, and L. L. Howell, "On the nomenclature, classification, and abstractions of compliant mechanisms," *Journal of Mechanical Design, Transactions of the ASME*, vol. 116, no. 1, pp. 270–279, 1994, doi: 10.1115/1.2919358.
- [2] L. L. Howell, *Compliant Mechanisms*. Wiley-Interscience Publications, 2001.
- [3] Y. Q. Yu, P. Zhou, and Q. P. Xu, "Kinematic and dynamic analysis of compliant mechanisms considering both lateral and axial deformations of flexural beams," *Proc Inst Mech Eng C J Mech Eng Sci*, 2019, doi: 10.1177/0954406218760956.
- [4] Y. Liu, Y. Zhang, and Q. Xu, "Design and Control of a Novel Compliant Constant-Force Gripper Based on Buckled Fixed-Guided Beams," *IEEE/ASME Transactions on Mechatronics*, 2017, doi: 10.1109/TMECH.2016.2614966.
- [5] T. Dao and S. Huang, "Design and Analysis of Flexible Slider Crank Mechanism," *World Academy of Science, Engineering and Technology International Journal of Aerospace and Mechanical Engineering*, 2014.
- [6] P. Bilancia, A. Geraci, and G. Berselli, "On the design of a long-stroke beam-based compliant mechanism providing quasi-constant force," in *ASME 2019 Conference on Smart Materials, Adaptive Structures and Intelligent Systems, SMASIS 2019*, 2019. doi: 10.1115/SMASIS2019-5519.
- [7] S. Pardeshi, S. Kandharkar, and B. Deshmukh, "Monolithic compliant slider crank mechanism for motion amplification," in *Materials Today: Proceedings*, 2017. doi: 10.1016/j.matpr.2017.02.007.



- [8] K. A. Tolman, E. G. Merriam, and L. L. Howell, "Compliant constant-force linear-motion mechanism," *Mech Mach Theory*, vol. 106, pp. 68–79, Dec. 2016, doi: 10.1016/j.mechmachtheory.2016.08.009.
- [9] V. Parlaktaş and E. Tanik, "Single piece compliant spatial slider-crank mechanism," *Mech Mach Theory*, 2014, doi: 10.1016/j.mechmachtheory.2014.06.007.
- [10] Ç. M. Tanik, E. Tanik, Y. Yazicioglu, and V. Parlaktaş, "On the analysis and design of a fully compliant large stroke slider-crank (rocker) mechanism," *Mechanical Sciences*, vol. 11, no. 1, pp. 29–38, 2020, doi: 10.5194/ms-11-29-2020.
- [11] B. P. Trease, Y. M. Moon, and S. Kota, "Design of large-displacement compliant joints," *Journal of Mechanical Design, Transactions of the ASME*, vol. 127, no. 4, pp. 788–798, Aug. 2005, doi: 10.1115/1.1900149.
- [12] T. S. Yang, P. J. Shih, and J. J. Lee, "Design of a spatial compliant translational joint," *Mech Mach Theory*, vol. 107, pp. 338–350, Jan. 2017, doi: 10.1016/j.mechmachtheory.2016.08.007.
- [13] J. van Eijk, "ON THE DESIGN OF PLATE-SPRING MECHANISMS.," 1985.
- [14] S. Awtar, A. H. Slocum, and E. Sevincer, "Characteristics of beam-based flexure modules," *Journal of Mechanical Design, Transactions of the ASME*, vol. 129, no. 6, pp. 625–639, 2007, doi: 10.1115/1.2717231.
- [15] Y. Li and Q. Xu, "Design and analysis of a totally decoupled flexure-based XY parallel micromanipulator," *IEEE Transactions on Robotics*, vol. 25, no. 3, 2009, doi: 10.1109/TRO.2009.2014130.
- [16] R. M. Panas, "Large displacement behavior of double parallelogram flexure mechanisms with underconstraint eliminators," *Precis Eng*, vol. 46, 2016, doi: 10.1016/j.precisioneng.2016.06.010.

- [17] R. M. Panas and J. B. Hopkins, "Eliminating Underconstraint in Double Parallelogram Flexure Mechanisms," *Journal of Mechanical Design, Transactions of the ASME*, vol. 137, no. 9, 2015, doi: 10.1115/1.4030773.
- [18] J. B. Hopkins and R. M. Panas, "A family of flexures that eliminate underconstraint in nested large-stroke flexure systems," in *Proceedings of the 13th International Conference of the European Society for Precision Engineering and Nanotechnology, EUSPEN 2013*, 2013, vol. 2.
- [19] L. L. Howell, S. P. Magleby, and B. M. Olsen, *Handbook of Compliant Mechanisms*. 2013. doi: 10.1002/9781118516485.
- [20] L. L. Howell and A. Midha, "A method for the design of compliant mechanisms with small-length flexural pivots," *Journal of Mechanical Design, Transactions of the ASME*, vol. 116, no. 1, 1994, doi: 10.1115/1.2919359.
- [21] I. Her, "Methodology for compliant mechanisms design," 1986.
- [22] A. Pandiyan and G. Arunkumar, "Design methods for compliant mechanisms used in new age industries-A review," *Journal of Applied Engineering Science*, vol. 14, no. 2. pp. 223–232, 2016. doi: 10.5937/jaes14-8229.
- [23] N. Lobontiu, J. S. N. Paine, E. Garcia, and M. Goldfarb, "Corner-filletted flexure hinges," *Journal of Mechanical Design, Transactions of the ASME*, vol. 123, no. 3, 2001, doi: 10.1115/1.1372190.
- [24] M. Goldfarb and J. E. Speich, "A well-behaved revolute flexure joint for compliant mechanism design," *Journal of Mechanical Design, Transactions of the ASME*, vol. 121, no. 3, 1999, doi: 10.1115/1.2829478.
- [25] S. T. Smith and D. C. Chetwynd, *Foundations of ultra-precision mechanism design*. 2017. doi: 10.1201/9781315272603.

- [26] J. B. Hopkins and M. L. Culpepper, "Synthesis of precision serial flexure systems using freedom and constraint topologies (FACT)," *Precis Eng*, vol. 35, no. 4, 2011, doi: 10.1016/j.precisioneng.2011.04.006.
- [27] J. van Eijk, "ON THE DESIGN OF PLATE-SPRING MECHANISMS.," 1985.

APPENDICES

A. CoC of Polypropylene

Sustaplast-Strasse 1 D-56112 Lahnstein/Germany Tel. +49 2621693-0 Fax +49 2621693170 Internet: www.sustaplast.de		 RÖCHLING Sustaplast
------------------------------------------------------------------------------------------------------------------------------	-----------------------------------------------------------------------------------	----------------------------------------------------------------------------------------------------------------------

Certificate 2.2 (EN 10 204)

CLIENTE/Client:	
VS. ORDINE/Your order-number:	
NR. ORDINE SUSTAPLAST/Order nr: Sustaplast	
DDT NR/delivery note nr.:	1730
FATTURA NR/invoice nr.:	1119

MATERIALE, DENOMINAZIONE/material, designation:	Susta ® PP-H
DIN EN ISO 1043 norm	PP-H
PRODUTTORE/manufacturer	Röchling Sustaplast KG
COLORE/colour	NATURALE/GRIGIO
FORMA/shape	ROD
DIMENSIONI/dimension	see above invoice
QUANTITA'/quantity	see above invoice

PROPRIETA' <i>properties</i>	UNITA' DI MISURA <i>measuring unit</i>	METODO DI PROVA <i>test method</i>	VALORI RILEVATI <i>value</i>
Pesi specifico/Density	g/cm ³	DIN EN ISO 1183-1	0,92
Resistenza alla trazione/Yield point	Mpa	DIN EN ISO 527	33
Allungamento a rottura/Elongation at break	%	DIN EN ISO 527	150
Modulo di elasticità /Modulus of elasticity	Mpa	DIN EN ISO 527	1.381
Prova di resilienza Charpy /notched impact strenght (Charpy)	KJ/m ²	ISO 179/1 eA/Pendel 1J	4
Prova di durezza con penetrazione/ball indentation hardness	Mpa	DIN EN ISO 2039	73
Durezza shore/ shore hardness	Skala D	DIN 53505	72
Indice di viscosità/viscosity number:	cm ³ /g	ISO 307/DIN 53728 T3	-
Indice di fluidità/melt flow rate MFR	g/10 min	DIN EN ISO 1133	-
Punto di fusione/Melting temperature	°C	ISO 11357	166

Ulteriori valori disponibili nel ns. catalogo "Caratteristiche tecniche"
You will find further data in our product information "Properties"

Röchling Sustaplast KG

Questo e' un certificato generato dal computer e non contiene firma in originale. I valori sopra riportati sono il risultato di esami non specifici, risultano da una media tra diverse misurazioni individuali e corrispondono alle nostre conoscenze odierne.

This is a computer generated certificate and does not contain a hand signed signature. The above mentioned values result from non-specific examination, they result from the average of many individual measurements and correspond to our today's knowledge.

